PHILOSOPHICAL TRANSACTIONS OF THE ROYAL SOCIETY A

rsta.royalsocietypublishing.org

Research

Cite this article: Hansen J, Sato M, Russell G, Kharecha P. 2013 Climate sensitivity, sea level and atmospheric carbon dioxide. Phil Trans R Soc A 371: 20120294.
http://dx.doi.org/10.1098/rsta.2012.0294

One contribution of 11 to a Discussion Meeting Issue 'Warm climates of the past—a lesson for the future?'.

Subject Areas:
climatology

Keywords:
climate, climate sensitivity, palaeoclimate, sea level

Author for correspondence:
James Hansen
e-mail: jimehansen@gmail.com

Electronic supplementary material is available at http://dx.doi.org/10.1098/rsta.2012.0294 or via http://rsta.royalsocietypublishing.org.

Royal Society Publishing
Informing the science of the future

Climate sensitivity, sea level and atmospheric carbon dioxide

James Hansen[1], Makiko Sato[1], Gary Russell[2] and Pushker Kharecha[1,2]

[1]The Earth Institute, Columbia University, New York, NY 10027, USA
[2]NASA Goddard Institute for Space Studies, New York, NY 10027, USA

Cenozoic temperature, sea level and CO_2 covariations provide insights into climate sensitivity to external forcings and sea-level sensitivity to climate change. Climate sensitivity depends on the initial climate state, but potentially can be accurately inferred from precise palaeoclimate data. Pleistocene climate oscillations yield a fast-feedback climate sensitivity of $3 \pm 1°C$ for a $4\,W\,m^{-2}$ CO_2 forcing if Holocene warming relative to the Last Glacial Maximum (LGM) is used as calibration, but the error (uncertainty) is substantial and partly subjective because of poorly defined LGM global temperature and possible human influences in the Holocene. Glacial-to-interglacial climate change leading to the prior (Eemian) interglacial is less ambiguous and implies a sensitivity in the upper part of the above range, i.e. 3–4°C for a $4\,W\,m^{-2}$ CO_2 forcing. Slow feedbacks, especially change of ice sheet size and atmospheric CO_2, amplify the total Earth system sensitivity by an amount that depends on the time scale considered. Ice sheet response time is poorly defined, but we show that the slow response and hysteresis in prevailing ice sheet models are exaggerated. We use a global model, simplified to essential processes, to investigate state dependence of climate sensitivity, finding an increased sensitivity towards warmer climates, as low cloud cover is diminished and increased water vapour elevates the tropopause. Burning all fossil fuels, we conclude, would make most of the planet uninhabitable by humans, thus calling into question strategies that emphasize adaptation to climate change.

1. Introduction

Humanity is now the dominant force driving changes in the Earth's atmospheric composition and climate [1]. The largest climate forcing today, i.e. the greatest imposed perturbation of the planet's energy balance [1,2], is the human-made increase in atmospheric greenhouse gases (GHGs), especially CO_2 from the burning of fossil fuels.

Earth's response to climate forcings is slowed by the inertia of the global ocean and the great ice sheets on Greenland and Antarctica, which require centuries, millennia or longer to approach their full response to a climate forcing. This long response time makes the task of avoiding dangerous human alteration of climate particularly difficult, because the human-made climate forcing is being imposed rapidly, with most of the current forcing having been added in just the past several decades. Thus, observed climate changes are only a partial response to the current climate forcing, with further response still 'in the pipeline' [3].

Climate models, numerical climate simulations, provide one way to estimate the climate response to forcings, but it is difficult to include realistically all real-world processes. Earth's palaeoclimate history allows empirical assessment of climate sensitivity, but the data have large uncertainties. These approaches are usually not fully independent, and the most realistic eventual assessments will be ones combining their greatest strengths.

We use the rich climate history of the Cenozoic era in the oxygen isotope record of ocean sediments to explore the relation of climate change with sea level and atmospheric CO_2, inferring climate sensitivity empirically. We use isotope data from Zachos *et al.* [4], which are improved over data used in our earlier study [5], and we improve our prescription for separating the effects of deep ocean temperature and ice volume in the oxygen isotope record as well as our prescription for relating deep ocean temperature to surface air temperature. Finally, we use an efficient climate model to expand our estimated climate sensitivities beyond the Cenozoic climate range to snowball Earth and runaway greenhouse conditions.

2. Overview of Cenozoic climate and our analysis approach

The Cenozoic era, the past 65.5 million years (Myr), provides a valuable perspective on climate [5,6] and sea-level change [7], and Cenozoic data help clarify our analysis approach. The principal dataset we use is the temporal variation of the oxygen isotope ratio ($\delta^{18}O$ relative to $\delta^{16}O$; figure 1*a* right-hand scale) in the shells of deep-ocean-dwelling microscopic shelled animals (foraminifera) in a near-global compilation of ocean sediment cores [4]. $\delta^{18}O$ yields an estimate of the deep ocean temperature (figure 1*b*), as discussed in §3. Note that coarse temporal resolution of $\delta^{18}O$ data in the intervals 7–17, 35–42 and 44–65 Myr reduces the apparent amplitude of glacial–interglacial climate fluctuations (see electronic supplementary material, figure S1). We use additional proxy measures of climate change to supplement the $\delta^{18}O$ data in our quantitative analyses.

Carbon dioxide is involved in climate change throughout the Cenozoic era, both as a climate forcing and as a climate feedback. Long-term Cenozoic temperature trends, the warming up to about 50 Myr before present (BP) and subsequent long-term cooling, are likely to be, at least in large part, a result of the changing natural source of atmospheric CO_2, which is volcanic emissions that occur mainly at continental margins due to plate tectonics (popularly 'continental drift'); tectonic activity also affects the weathering sink for CO_2 by exposing fresh rock. The CO_2 tectonic source grew from 60 to 50 Myr BP as India subducted carbonate-rich ocean crust while moving through the present Indian Ocean prior to its collision with Asia about 50 Myr BP [8], causing atmospheric CO_2 to reach levels of the order of 1000 ppm at 50 Myr BP [9]. Since then, atmospheric CO_2 declined as the Indian and Atlantic Oceans have been major depocentres for carbonate and organic sediments while subduction of carbonate-rich crust has been limited mainly to small regions near Indonesia and Central America [10], thus allowing CO_2 to decline to levels as low as 170 ppm during recent glacial periods [11]. A climate forcing due to a CO_2 change from 1000 to 170 ppm is more than 10 W m^{-2}, which compares with forcings of the order of 1 W m^{-2} for

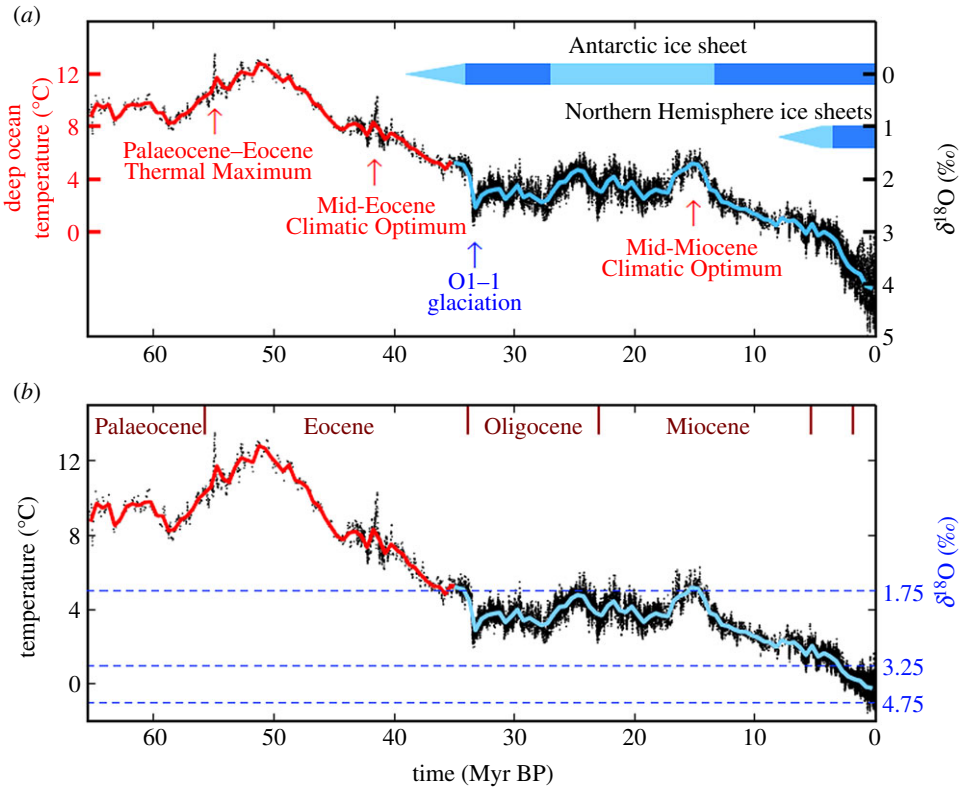

Figure 1. (*a*) Global deep ocean $\delta^{18}O$ from Zachos *et al.* [4] and (*b*) estimated deep ocean temperature based on the prescription in our present paper. Black data points are five-point running means of the original temporal resolution; red and blue curves have a 500 kyr resolution. Coarse temporal sampling reduces the amplitude of glacial–interglacial oscillations in the intervals 7–17, 35–42 and 44–65 Myr BP.

competing climate forcings during the Cenozoic era [5], specifically long-term change of solar irradiance and change of planetary albedo (reflectance) owing to the overall minor displacement of continents in that era.

Superimposed on the long-term trends are occasional global warming spikes, 'hyperthermals', most prominently the Palaeocene–Eocene Thermal Maximum (PETM) at approximately 56 Myr BP [12] and the Mid-Eocene Climatic Optimum at approximately 42 Myr BP [13], coincident with large temporary increases of atmospheric CO_2. The most studied hyperthermal, the PETM, caused global warming of at least 5°C coincident with injection of a likely 4000–7000 Gt of isotopically light carbon into the atmosphere and ocean [14]. The size of the carbon injection is estimated from changes in the stable carbon isotope ratio $^{13}C/^{12}C$ in sediments and from ocean acidification implied by changes in the ocean depth below which carbonate dissolution occurred.

The potential carbon source for hyperthermal warming that received most initial attention was methane hydrates on continental shelves, which could be destabilized by sea floor warming [15]. Alternative sources include release of carbon from Antarctic permafrost and peat [16]. Regardless of the carbon source(s), it has been shown that the hyperthermals were astronomically paced, spurred by coincident maxima in the Earth's orbit eccentricity and spin axis tilt [17], which increased high-latitude insolation and warming. The PETM was followed by successively weaker astronomically paced hyperthermals, suggesting that the carbon source(s) partially recharged in the interim [18]. A high temporal resolution sediment core from the New Jersey continental shelf [19] reveals that PETM warming in at least that region began about 3000 years prior to a massive release of isotopically light carbon. This lag and climate simulations [20] that produce

large warming at intermediate ocean depths in response to initial surface warming are consistent with the concept of a methane hydrate role in hyperthermal events.

The hyperthermals confirm understanding about the long recovery time of the Earth's carbon cycle [21] and reveal the potential for threshold or 'tipping point' behaviour with large amplifying climate feedback in response to warming [22]. One implication is that if humans burn most of the fossil fuels, thus injecting into the atmosphere an amount of CO_2 at least comparable to that injected during the PETM, the CO_2 would stay in the surface carbon reservoirs (atmosphere, ocean, soil, biosphere) for tens of thousands of years, long enough for the atmosphere, ocean and ice sheets to fully respond to the changed atmospheric composition. In addition, there is the potential that global warming from fossil fuel CO_2 could spur release of CH_4 and CO_2 from methane hydrates or permafrost. Carbon release during the hyperthermals required several thousand years, but that long injection time may have been a function of the pace of the astronomical forcing, which is much slower than the pace of fossil fuel burning.

The Cenozoic record also reveals the amplification of climate change that occurs with growth or decay of ice sheets, as is apparent at about 34 Myr BP when the Earth became cool enough for large-scale glaciation of Antarctica and in the most recent 3–5 Myr with the growth of Northern Hemisphere ice sheets. Global climate fluctuated in the 20 Myr following Antarctic glaciation with warmth during the Mid-Miocene Climatic Optimum (MMCO, 15 Myr BP) possibly comparable to that at 34 Myr BP, as, for example, Germany became warm enough to harbour snakes and crocodiles that require an annual temperature of about 20°C or higher and a winter temperature more than 10°C [23]. Antarctic vegetation in the MMCO implies a summer temperature of approximately 11°C warmer than today [24] and annual sea surface temperatures ranging from 0°C to 11.5°C [25].

Superimposed on the long-term trends, in addition to occasional hyperthermals, are continual high-frequency temperature oscillations, which are apparent in figure 1 after 34 Myr BP, when the Earth became cold enough for a large ice sheet to form on Antarctica, and are still more prominent during ice sheet growth in the Northern Hemisphere. These climate oscillations have dominant periodicities, ranging from about 20 to 400 kyr, that coincide with variations in the Earth's orbital elements [26], specifically the tilt of the Earth's spin axis, the eccentricity of the orbit and the time of year when the Earth is closest to the Sun. The slowly changing orbit and tilt of the spin axis affect the seasonal distribution of insolation [27], and thus the growth and decay of ice sheets, as proposed by Milankovitch [28]. Atmospheric CO_2, CH_4 and N_2O have varied almost synchronously with global temperature during the past 800 000 years for which precise data are available from ice cores, the GHGs providing an amplifying feedback that magnifies the climate change instigated by orbit perturbations [29–31].

Ocean and atmosphere dynamical effects have been suggested as possible causes of some climate change within the Cenozoic era; for example, topographical effects of mountain building [32], closing of the Panama Seaway [33] or opening of the Drake Passage [34]. Climate modelling studies with orographic changes confirm significant effects on monsoons and on Eurasian temperature [35]. Modelling studies indicate that closing of the Panama Seaway results in a more intense Atlantic thermohaline circulation, but only small effects on Northern Hemisphere ice sheets [36]. Opening of the Drake Passage surely affected ocean circulation around Antarctica, but efforts to find a significant effect on global temperature have relied on speculation about possible effects on atmospheric CO_2 [37]. Overall, there is no strong evidence that dynamical effects are a major direct contributor to Cenozoic global temperature change.

We hypothesize that the global climate variations of the Cenozoic (figure 1) can be understood and analysed via slow temporal changes in Earth's energy balance, which is a function of solar irradiance, atmospheric composition (specifically long-lived GHGs) and planetary surface albedo. Using measured amounts of GHGs during the past 800 000 years of glacial–interglacial climate oscillations and surface albedo inferred from sea-level data, we show that a single empirical 'fast-feedback' climate sensitivity can account well for the global temperature change over that range of climate states. It is certain that over a large climate range climate sensitivity must become a strong function of the climate state, and thus we use a simplified climate model to investigate

the dependence of climate sensitivity on the climate state. Finally, we use our estimated state-dependent climate sensitivity to infer Cenozoic CO_2 change and compare this with proxy CO_2 data, focusing on the Eocene climatic optimum, the Oligocene glaciation, the Miocene optimum and the Pliocene.

3. Deep ocean temperature and sea level in the Cenozoic era

The $\delta^{18}O$ stable isotope ratio was the first palaeothermometer, proposed by Urey [38] and developed especially by Emiliani [39]. There are now several alternative proxy measures of ancient climate change, but the $\delta^{18}O$ data (figure 1*a*) of Zachos *et al.* [4], a conglomerate of the global ocean sediment cores, is well suited for our purpose as it covers the Cenozoic era with good temporal resolution. There are large, even dominant, non-climatic causes of $\delta^{18}O$ changes over hundreds of millions of years [40], but non-climatic change may be small in the past few hundred million years [41] and is generally neglected in Cenozoic climate studies. The principal difficulty in using the $\delta^{18}O$ record to estimate global deep ocean temperature, in the absence of non-climatic change, is that $\delta^{18}O$ is affected by the global ice mass as well as the deep ocean temperature.

We make a simple estimate of global sea-level change for the Cenozoic era using the near-global $\delta^{18}O$ compilation of Zachos *et al.* [4]. More elaborate and accurate approaches, including use of models, will surely be devised, but comparison of our result with other approaches is instructive regarding basic issues such as the vulnerability of today's ice sheets to near-term global warming and the magnitude of hysteresis effects in ice sheet growth and decay.

During the Early Cenozoic, between 65.5 and 35 Myr BP, the Earth was so warm that there was little ice on the planet and the deep ocean temperature is approximated by [6]

$$T_{do}\,(^{\circ}C) = -4\delta^{18}O + 12 \quad (\text{for } \delta^{18}O < 1.75). \tag{3.1}$$

Hansen *et al.* [5] made the approximation that, as the Earth became colder and continental ice sheets grew, further increase in $\delta^{18}O$ was due, in equal parts, to deep ocean temperature change and ice mass change,

$$T_{do}\,(^{\circ}C) = -2(\delta^{18}O - 4.25) \quad (\text{for } \delta^{18}O > 1.75). \tag{3.2}$$

Equal division of the $\delta^{18}O$ change into temperature change and ice volume change was suggested by comparing $\delta^{18}O$ at the endpoints of the climate change from the nearly ice-free planet at 35 Myr BP (when $\delta^{18}O$ approx. 1.75) with the Last Glacial Maximum (LGM), which peaked approximately 20 kyr BP. The change of $\delta^{18}O$ between these two extreme climate states (approx. 3) is twice the change of $\delta^{18}O$ due to temperature change alone (approx. 1.5), with the temperature change based on the linear relation (3.1) and estimates of $T_{do} \sim 5^{\circ}C$ at 35 Myr BP (figure 1) and approximately $-1^{\circ}C$ at the LGM [42].

This approximation can easily be made more realistic. Although ice volume and deep ocean temperature changes contributed comparable amounts to $\delta^{18}O$ change on average over the full range from 35 Myr to 20 kyr BP, the temperature change portion of the $\delta^{18}O$ change must decrease as the deep ocean temperature approaches the freezing point [43]. The rapid increase in $\delta^{18}O$ in the past few million years was associated with the appearance of Northern Hemisphere ice sheets, symbolized by the dark blue bar in figure 1*a*.

The sea-level change between the LGM and Holocene was approximately 120 m [44,45]. Thus, two-thirds of the 180 m sea-level change between the ice-free planet and the LGM occurred with formation of Northern Hemisphere ice (and probably some increased volume of Antarctic ice). Thus, rather than taking the 180 m sea-level change between the nearly ice-free planet of 34 Myr BP and the LGM as being linear over the entire range (with 90 m for $\delta^{18}O < 3.25$ and 90 m for $\delta^{18}O > 3.25$), it is more realistic to assign 60 m of sea-level change to $\delta^{18}O$ 1.75–3.25 and 120 m to $\delta^{18}O > 3.25$. The total deep ocean temperature change of 6°C for the change of $\delta^{18}O$ from 1.75

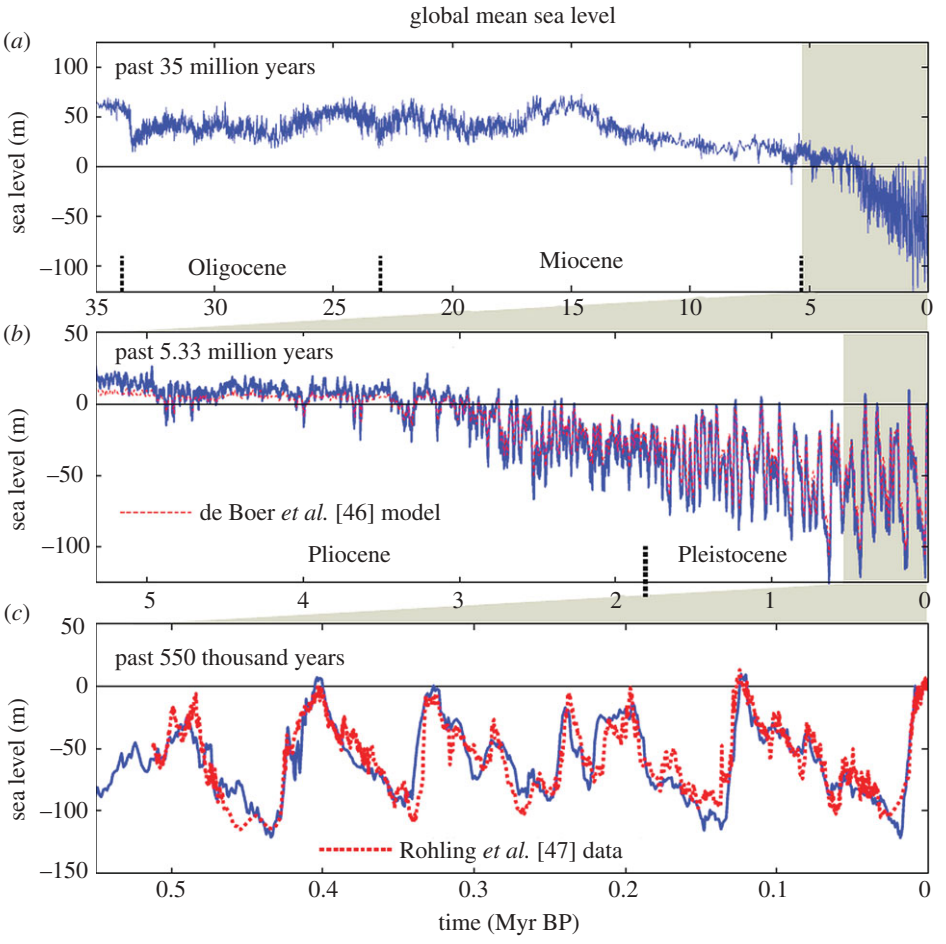

Figure 2. (*a–c*) Sea level from equations (3.3) and (3.4) using δ^{18}O data of Zachos *et al.* [4], compared in (*b*) with ice sheet model results of de Boer *et al.* [46] and in (*c*) with the sea-level analysis of Rohling *et al.* [47].

to 4.75 is then divided two-thirds (4°C) for the δ^{18}O range 1.75–3.25 and 2°C for the δ^{18}O range 3.25–4.75. Algebraically,

$$\mathrm{SL\ (m)} = 60 - 40(\delta^{18}\mathrm{O} - 1.75) \quad (\text{for } \delta^{18}\mathrm{O} < 3.25), \tag{3.3}$$

$$\mathrm{SL\ (m)} = -120\frac{\delta^{18}\mathrm{O} - 3.25}{1.65} \quad (\text{for } \delta^{18}\mathrm{O} > 3.25), \tag{3.4}$$

$$T_{\mathrm{do}}\ (^{\circ}\mathrm{C}) = 5 - 8\frac{\delta^{18}\mathrm{O} - 1.75}{3} \quad (\text{for } \delta^{18}\mathrm{O} < 3.25) \tag{3.5}$$

and

$$T_{\mathrm{do}}\ (^{\circ}\mathrm{C}) = 1 - 4.4\frac{\delta^{18}\mathrm{O} - 3.25}{3} \quad (\text{for } \delta^{18}\mathrm{O} > 3.25), \tag{3.6}$$

where SL is the sea level and its zero point is the Late Holocene level. The coefficients in equations (3.4) and (3.6) account for the fact that the mean LGM value of δ^{18}O is approximately 4.9. The resulting deep ocean temperature is shown in figure 1*b* for the full Cenozoic era.

Sea level from equations (3.3) and (3.4) is shown by the blue curves in figure 2, including comparison (figure 2*c*) with the Late Pleistocene sea-level record of Rohling *et al.* [47], which is based on analysis of Red Sea sediments, and comparison (figure 2*b*) with the sea-level chronology of de Boer *et al.* [46], which is based on ice sheet modelling with the δ^{18}O data of Zachos *et al.* [4] as a principal input driving the ice sheet model. Comparison of our result with that of de Boer

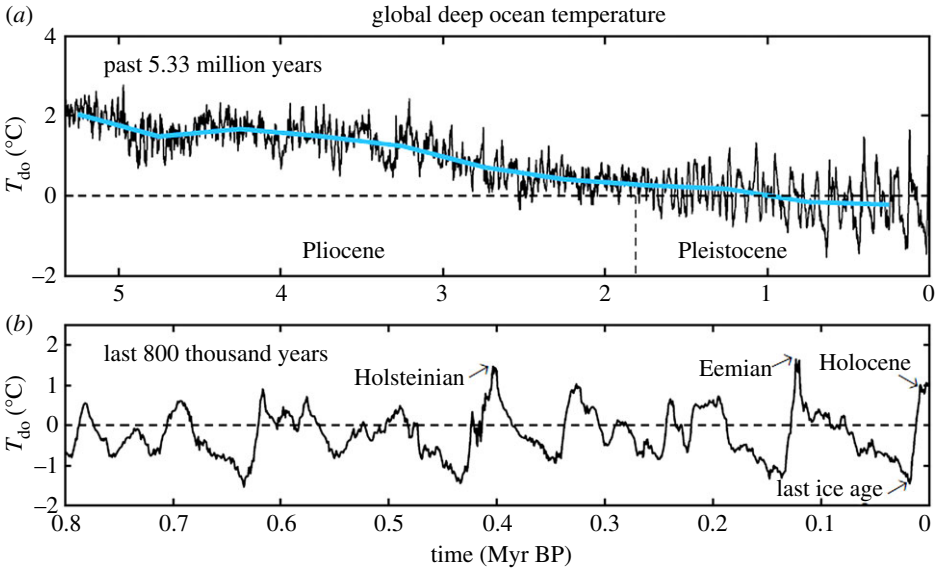

Figure 3. Deep ocean temperature in (*a*) the Pliocene and Pleistocene and (*b*) the last 800 000 years. High-frequency variations (black) are five-point running means of the original data [4], whereas the blue curve has a 500 kyr resolution. The deep ocean temperature for the entire Cenozoic era is in figure 1*b*.

et al. [46] for the other periods of figure 2 is included in the electronic supplementary material, where we also make available our numerical data. Deep ocean temperature from equations (3.5) and (3.6) is shown for the Pliocene and Pleistocene in figure 3 and for the entire Cenozoic era in figure 1.

Differences between our inferred sea-level chronology and that from the ice sheet model [46] are relevant to the assessment of the potential danger to humanity from future sea-level rise. Our estimated sea levels have reached +5 to 10 m above the present sea level during recent interglacial periods that were barely warmer than the Holocene, whereas the ice sheet model yields maxima at most approximately 1 m above the current sea level. We find the Pliocene sea level varying between about +20 m and −50 m, with the Early Pliocene averaging about +15 m; the ice sheet model has a less variable sea level with the Early Pliocene averaging about +8 m. A 15 m sea-level rise implies that the East Antarctic ice sheet as well as West Antarctica and Greenland ice were unstable at a global temperature no higher than those projected to occur this century [1,48].

How can we interpret these differences, and what is the merit of our simple $\delta^{18}O$ scaling? Ice sheet models constrained by multiple observations may eventually provide our best estimate of sea-level change, but as yet models are primitive. Hansen [49,50] argues that real ice sheets are more responsive to climate change than is found in most ice sheet models. Our simple scaling approximation implicitly assumes that ice sheets are sufficiently responsive to climate change that hysteresis is not a dominant effect; in other words, ice volume on millennial time scales is a function of temperature and does not depend much on whether the Earth is in a warming or cooling phase. Thus, our simple transparent calculation may provide a useful comparison with geological data for sea-level change and with results of ice sheet models.

We cannot *a priori* define accurately the error in our sea-level estimates, but we can compare with geological data in specific cases as a check on reasonableness. Our results (figure 2) yield two instances in the past million years when sea levels have reached heights well above the current sea level: +9.8 m in the Eemian (approx. 120 kyr BP, also known as Marine Isotope Stage 5e or MIS-5e) and +7.1 m in the Holsteinian (approx. 400 kyr BP, also known as MIS-11). Indeed, these are the two interglacial periods in the Late Pleistocene that traditional geological methods identify

as probably having a sea level exceeding that in the Holocene. Geological evidence, mainly coral reefs on tectonically stable coasts, was described in the review of Overpeck *et al.* [51] as favouring an Eemian maximum of +4 to more than 6 m. Rohling *et al.* [52] cite many studies concluding that the mean sea level was 4–6 m above the current sea level during the warmest portion of the Eemian, 123–119 kyr BP; note that several of these studies suggest Eemian sea-level fluctuations up to +10 m, and provide the first continuous sea-level data supporting rapid Eemian sea-level fluctuations. Kopp *et al.* [53] made a statistical analysis of data from a large number of sites, concluding that there was a 95% probability that the Eemian sea level reached at least +6.6 m with a 67% probability that it exceeded 8 m.

The Holsteinian sea level is more difficult to reconstruct from geological data because of its age, and there has been a long-standing controversy concerning a substantial body of geological shoreline evidence for a +20 m Late Holsteinian sea level that Hearty and co-workers have found on numerous sites [54,55] (numerous pros and cons are contained in the references provided in our present paragraph). Rohling *et al.* [56] note that their temporally continuous Red Sea record 'strongly supports the MIS-11 sea level review of Bowen [57], which also places MIS-11 sea level within uncertainties at the present-day level'. This issue is important because both ice core data [29] and ocean sediment core data (see below) indicate that the Holsteinian period was only moderately warmer than the Holocene with similar Earth orbital parameters. We suggest that the resolution of this issue is consistent with our estimate of the approximately +7 m Holsteinian global sea level, and is provided by Raymo & Mitrovica [58], who pointed out the need to make a glacial isostatic adjustment (GIA) correction for post-glacial crustal subsidence at the places where Hearty and others deduced local sea-level change. The uncertainties in GIA modelling led Raymo & Mitrovica [58] to conclude that the peak Holsteinian global sea level was in the range of +6 to 13 m relative to the present. Thus, it seems to us, there is a reasonable resolution of the long-standing Holsteinian controversy, with substantial implications for humanity, as discussed in later sections.

We now address differences between our sea-level estimates and those from ice sheet models. We refer to both the one-dimensional ice sheet modelling of de Boer *et al.* [46], which was used to calculate sea level for the entire Cenozoic era, and the three-dimensional ice sheet model of Bintanja *et al.* [59], which was used for simulations of the past million years. The differences most relevant to humanity occur in the interglacial periods slightly warmer than the Holocene, including the Eemian and Hosteinian, as well as the Pliocene, which may have been as warm as projected for later this century. Both the three-dimensional model of Bintanja *et al.* [59] and the one-dimensional model of de Boer *et al.* [46] yield maximum Eemian and Hosteinian sea levels of approximately 1 m relative to the Holocene. de Boer *et al.* [46] obtain approximately +8 m for the Early Pliocene, which compares with our approximately +15 m.

These differences reveal that the modelled ice sheets are less susceptible to change in response to global temperature variation than our $\delta^{18}O$ analysis. Yet the ice sheet models do a good job of reproducing the sea-level change for climates colder than the Holocene, as shown in figure 2 and electronic supplementary material, figure S2. One possibility is that the ice sheet models are too lethargic for climates warmer than the Holocene. Hansen & Sato [60] point out the sudden change in the responsiveness of the ice sheet model of Bintanja *et al.* [59] when the sea level reaches today's level (figs 3 and 4 of Hansen & Sato [60]) and they note that the empirical sea-level data provide no evidence of such a sudden change. The explanation conceivably lies in the fact that the models have many parameters and their operation includes use of 'targets' [46] that affect the model results, because these choices might yield different results for warmer climates than the results for colder climates. Because of the potential that model development choices might be influenced by expectations of a 'correct' result, it is useful to have estimates independent of the models based on alternative assumptions.

Note that our approach also involves 'targets' based on expected behaviour, albeit simple transparent ones. Our two-legged linear approximation of the sea level (equations (3.3) and (3.4)) assumes that the sea level in the LGM was 120 m lower than today and that the sea level was 60 m higher than today 35 Myr BP. This latter assumption may need to be adjusted if glaciers and ice

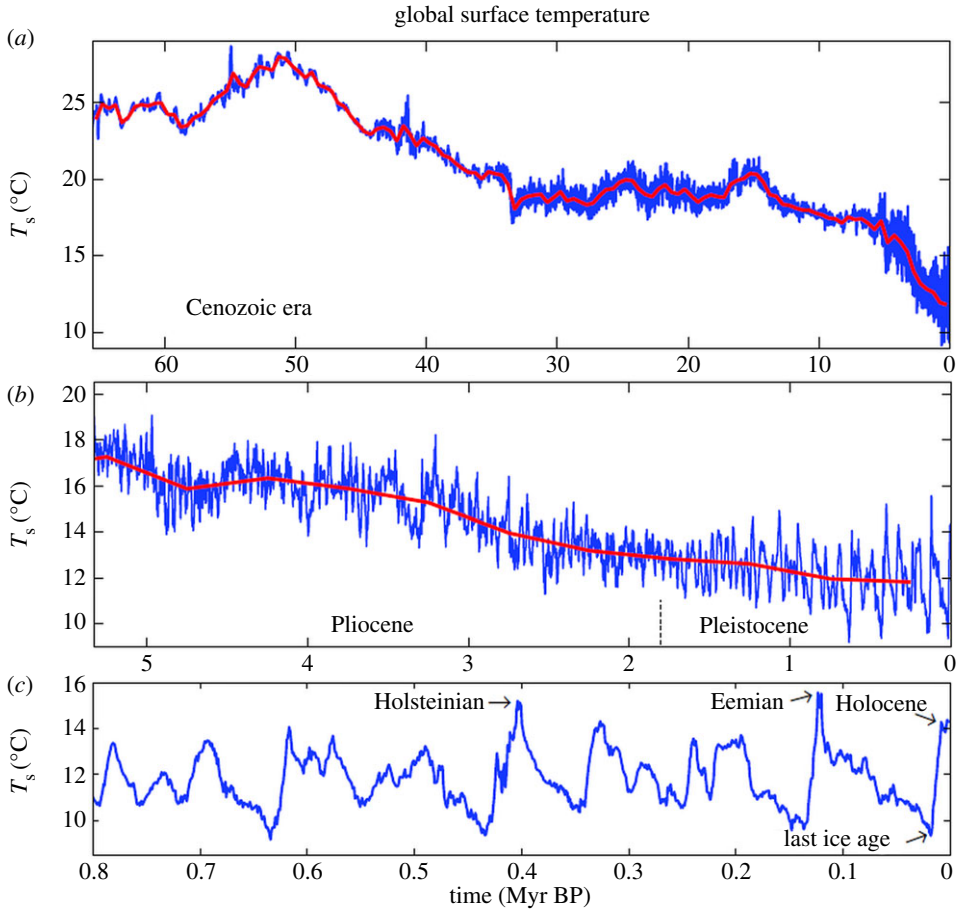

Figure 4. (*a–c*) Surface temperature estimate for the past 65.5 Myr, including an expanded time scale for (*b*) the Pliocene and Pleistocene and (*c*) the past 800 000 years. The red curve has a 500 kyr resolution. Data for this and other figures are available in the electronic supplementary material.

caps in the Eocene had a volume of tens of metres of sea level. However, Miller *et al.* [61] conclude that there was a sea level fall of approximately 55 m at the Eocene–Oligocene transition, consistent with our assumption that Eocene ice probably did not contain more than approximately 10 m of sea level.

Real-world data for the Earth's sea-level history ultimately must provide assessment of sea-level sensitivity to climate change. A recent comprehensive review [7] reveals that there are still wide uncertainties about the Earth's sea-level history that are especially large for time scales of tens of millions of years or longer, which is long enough for substantial changes in the shape and volume of ocean basins. Gasson *et al.* [7] plot regional (New Jersey) sea level (their fig. 14) against the deep ocean temperature inferred from the magnesium/calcium ratio (Mg/Ca) of deep ocean foraminifera [62], finding evidence for a nonlinear sea-level response to temperature roughly consistent with the modelling of de Boer *et al.* [46]. Sea-level change is limited for Mg/Ca temperatures up to about 5°C above current values, whereupon a rather abrupt sea-level rise of several tens of metres occurs, presumably representing the loss of Antarctic ice. However, the uncertainty in the reconstructed sea level is tens of metres and the uncertainty in the Mg/Ca temperature is sufficient to encompass the result from our $\delta^{18}O$ prescription, which has comparable contributions of ice volume change and deep ocean temperature change at the Late Eocene glaciation of Antarctica.

Furthermore, the potential sea-level rise of most practical importance is the first 15 m above the Holocene level. It is such 'moderate' sea-level change for which we particularly question the projections implied by current ice sheet models. Empirical assessment depends upon real-world sea-level data in periods warmer than the Holocene. There is strong evidence, discussed above, that the sea level was several metres higher in recent warm interglacial periods, consistent with our data interpretation. The Pliocene provides data extension to still warmer climates. Our interpretation of δ^{18}O data suggests that Early Pliocene sea-level change (due to ice volume change) reached about +15 m, and it also indicates sea-level fluctuations as large as 20–40 m. Sea-level data for Mid-Pliocene warm periods, of comparable warmth to average Early Pliocene conditions (figure 3), suggest sea heights as great as +15–25 m [63,64]. Miller *et al.* [61] find a Pliocene sea-level maximum of 22 ± 10 m (95% confidence). GIA creates uncertainty in sea-level reconstructions based on shoreline geological data [65], which could be reduced via appropriately distributed field studies. Dwyer & Chandler [64] separate Pliocene ice volume and temperature in deep ocean δ^{18}O via ostracode Mg/Ca temperatures, finding sea-level maxima and oscillations comparable to our results. Altogether, the empirical data provide strong evidence against the lethargy and strong hysteresis effects of at least some ice sheet models.

4. Surface air temperature change

The temperature of most interest to humanity is the surface air temperature. A record of past global surface temperature is required for empirical inference of global climate sensitivity. Given that climate sensitivity can depend on the initial climate state and on the magnitude and sign of the climate forcing, a continuous record of global temperature over a wide range of climate states would be especially useful. Because of the singularly rich climate story in Cenozoic deep ocean δ^{18}O (figure 1), unrivalled in detail and self-consistency by alternative climate proxies, we use deep ocean δ^{18}O to provide the fine structure of Cenozoic temperature change. We use surface temperature proxies from the LGM, the Pliocene and the Eocene to calibrate and check the relation between deep ocean and surface temperature change.

The temperature signal in deep ocean δ^{18}O refers to the sea surface where cold dense water formed and sank to the ocean bottom, the principal location of deep water formation being the Southern Ocean. Empirical data and climate models concur that surface temperature change is generally amplified at high latitudes, which tends to make temperature change at the site of deep water formation an overestimate of global temperature change. Empirical data and climate models also concur that surface temperature change is amplified over land areas, which tends to make temperature change at the site of deep water an underestimate of the global temperature. Hansen *et al.* [5] and Hansen & Sato [60] noted that these two factors were substantially offsetting, and thus they made the assumption that benthic foraminifera provide a good approximation of global mean temperature change for most of the Cenozoic era.

However, this approximation breaks down in the Late Cenozoic for two reasons. First, the deep ocean and high-latitude surface ocean where deep water forms are approaching the freezing point in the Late Cenozoic. As the Earth's surface cools further, cold conditions spread to lower latitudes but polar surface water and the deep ocean cannot become much colder, and thus the benthic foraminifera record a temperature change smaller than the global average surface temperature change [43]. Second, the last 5.33 Myr of the Cenozoic, the Pliocene and Pleistocene, was the time that global cooling reached a degree such that large ice sheets could form in the Northern Hemisphere. When a climate forcing, or a slow climate feedback such as ice sheet formation, occurs in one hemisphere, the temperature change is much larger in the hemisphere with the forcing (cf. examples in Hansen *et al.* [66]). Thus, cooling during the last 5.33 Myr in the Southern Ocean site of deep water formation was smaller than the global average cooling.

We especially want our global surface temperature reconstruction to be accurate for the Pliocene and Pleistocene because the global temperature changes that are expected by the end of this century, if humanity continues to rapidly change atmospheric composition, are of a magnitude comparable to climate change in those epochs [1,48]. Fortunately, sufficient

information is available on surface temperature change in the Pliocene and Pleistocene to allow us to scale the deep ocean temperature change by appropriate factors, thus retaining the temporal variations in the δ^{18}O while also having a realistic magnitude for the total temperature change over these epochs.

Pliocene temperature is known quite well because of a long-term effort to reconstruct the climate conditions during the Mid-Pliocene warm period (3.29–2.97 Myr BP) and a coordinated effort to numerically simulate the climate by many modelling groups ([67] and papers referenced therein). The reconstructed Pliocene climate used data for the warmest conditions found in the Mid-Pliocene period, which would be similar to average conditions in the Early Pliocene (figure 3). These boundary conditions were used by eight modelling groups to simulate Pliocene climate with atmospheric general circulation models. Although atmosphere–ocean models have difficulty replicating Pliocene climate, atmospheric models forced by specified surface boundary conditions are expected to be capable of calculating global surface temperature with reasonable accuracy. The eight global models yield Pliocene global warming of 3 ± 1°C relative to the Holocene [68]. This Pliocene warming is an amplification by a factor of 2.5 of the deep ocean temperature change.

Similarly, for the reasons given above, the deep ocean temperature change of 2.25°C between the Holocene and the LGM is surely an underestimate of the surface air temperature change. Unfortunately, there is a wide range of estimates for LGM cooling, approximately 3–6°C, as discussed in §6. Thus, we take 4.5°C as our best estimate for LGM cooling, implying an amplification of surface temperature change by a factor of two relative to deep ocean temperature change for this climate interval.

We obtain an absolute temperature scale using the Jones *et al*. [69] estimate of 14°C as the global mean surface temperature for 1961–1990, which corresponds to approximately 13.9°C for the 1951–1980 base period that we normally use [70] and approximately 14.4°C for the first decade of the twenty-first century. We attach the instrumental temperature record to the palaeo data by assuming that the first decade of the twenty-first century exceeds the Holocene mean by 0.25 ± 0.25°C. Global temperature probably declined over the past several millennia [71], but we suggest that warming of the past century has brought global temperature to a level that now slightly exceeds the Holocene mean, judging from sea-level trends and ice sheet mass loss. Sea level is now rising 3.1 mm per year or 3.1 m per millennium [72], an order of magnitude faster than the rate during the past several thousand years, and Greenland and Antarctica are losing mass at accelerating rates [73,74]. Our assumption that global temperature passed the Holocene mean a few decades ago is consistent with the rapid change of ice sheet mass balance in the past few decades [75]. The above concatenation of instrumental and palaeo records yields a Holocene mean of 14.15°C and Holocene maximum (from five-point smoothed δ^{18}O) of 14.3°C at 8.6 kyr BP.

Given a Holocene temperature of 14.15°C and LGM cooling of 4.5°C, the Early Pliocene mean temperature 3°C warmer than the Holocene leads to the following prescription:

$$T_s\ (^\circ\mathrm{C}) = 2 \times T_{do} + 12.25^\circ\mathrm{C} \quad \text{(Pleistocene)} \tag{4.1}$$

and

$$T_s\ (^\circ\mathrm{C}) = 2.5 \times T_{do} + 12.15^\circ\mathrm{C} \quad \text{(Pliocene)}. \tag{4.2}$$

This prescription yields a maximum Eemian temperature of 15.56°C, which is approximately 1.4°C warmer than the Holocene mean and approximately 1.8°C warmer than the 1880–1920 mean. Clark & Huybers [76] fit a polynomial to proxy temperatures for the Eemian, finding warming as much as +5°C at high northern latitudes but global warming of +1.7°C 'relative to the present interglacial before industrialization'. Other analyses of Eemian data find global sea surface temperature warmer than the Late Holocene by 0.7 ± 0.6°C [77] and all-surface warming of 2°C [78], all in reasonable accord with our prescription.

Our first estimate of global temperature for the remainder of the Cenozoic assumes that $\Delta T_s = \Delta T_{do}$ prior to 5.33 Myr BP, i.e. prior to the Plio-Pleistocene, which yields a peak T_s of approximately 28°C at 50 Myr BP (figure 4). This is at the low end of the range of current

multi-proxy measures of sea surface temperature for the Early Eocene Climatic Optimum (EECO) [79–81]. Climate models are marginally able to reproduce this level of Eocene warmth, but the models require extraordinarily high CO_2 levels, for example 2240–4480 ppm [82] and 2500–6500 ppm [83], and the quasi-agreement between data and models requires an assumption that some of the proxy temperatures are biased towards summer values. Moreover, taking the proxy sea surface temperature data for the peak Eocene period (55–48 Myr BP) at face value yields a global temperature of 33–34°C (fig. 3 of Bijl *et al.* [84]), which would require an even larger CO_2 amount with the same climate models. Thus, below we also consider the implications for climate sensitivity of an assumption that $\Delta T_s = 1.5 \times \Delta T_{do}$ prior to 5.33 Myr BP, which yields T_s approximately 33°C at 50 Myr BP (see electronic supplementary material, figure S3).

5. Climate sensitivity

Climate sensitivity (S) is the equilibrium global surface temperature change (ΔT_{eq}) in response to a specified unit forcing after the planet has come back to energy balance,

$$S = \frac{\Delta T_{eq}}{F}, \tag{5.1}$$

i.e. climate sensitivity is the eventual (equilibrium) global temperature change per unit forcing. Climate sensitivity depends upon climate feedbacks, the many physical processes that come into play as climate changes in response to a forcing. Positive (amplifying) feedbacks increase the climate response, whereas negative (diminishing) feedbacks reduce the response.

We usually discuss climate sensitivity in terms of a global mean temperature response to a $4\,W\,m^{-2}$ CO_2 forcing. One merit of this standard forcing is that its magnitude is similar to an anticipated near-term human-made climate forcing, thus avoiding the need to continually scale the unit sensitivity to achieve an applicable magnitude. A second merit is that the efficacy of forcings varies from one forcing mechanism to another [66]; so it is useful to use the forcing mechanism of greatest interest. Finally, the $4\,W\,m^{-2}$ CO_2 forcing avoids the uncertainty in the exact magnitude of a doubled CO_2 forcing [1,48] estimate of $3.7\,W\,m^{-2}$ for doubled CO_2, whereas Hansen *et al.* [66] obtain $4.1\,W\,m^{-2}$, as well as problems associated with the fact that a doubled CO_2 forcing varies as the CO_2 amount changes (the assumption that each CO_2 doubling has the same forcing is meant to approximate the effect of CO_2 absorption line saturation, but actually the forcing per doubling increases as CO_2 increases [66,85]).

Climate feedbacks are the core of the climate problem. Climate feedbacks can be confusing, because in climate analyses what is sometimes a climate forcing is at other times a climate feedback. A CO_2 decrease from, say, approximately 1000 ppm in the Early Cenozoic to 170–300 ppm in the Pleistocene, caused by shifting plate tectonics, is a climate forcing, a perturbation of the Earth's energy balance that alters the temperature. Glacial–interglacial oscillations of the CO_2 amount and ice sheet size are both slow climate feedbacks, because glacial–interglacial climate oscillations largely are instigated by insolation changes as the Earth's orbit and tilt of its spin axis change, with the climate change then amplified by a nearly coincident change of the CO_2 amount and the surface albedo. However, for the sake of analysis, we can also choose and compare periods that are in quasi-equilibrium, periods during which there was little change of the ice sheet size or the GHG amount. For example, we can compare conditions averaged over several millennia in the LGM with mean Holocene conditions. The Earth's average energy imbalance within each of these periods had to be a small fraction of $1\,W\,m^{-2}$. Such a planetary energy imbalance is very small compared with the boundary condition 'forcings', such as changed GHG amount and changed surface albedo that maintain the glacial-to-interglacial climate change.

(a) Fast-feedback sensitivity: Last Glacial Maximum–Holocene

The average fast-feedback climate sensitivity over the LGM–Holocene range of climate states can be assessed by comparing estimated global temperature change and climate forcing change

between those two climate states [3,86]. The appropriate climate forcings are the changes in long-lived GHGs and surface properties on the planet. Fast feedbacks include water vapour, clouds, aerosols and sea ice changes.

This fast-feedback sensitivity is relevant to estimating the climate impact of human-made climate forcings, because the size of ice sheets is not expected to change significantly in decades or even in a century and GHGs can be specified as a forcing. GHGs change in response to climate change, but it is common to include these feedbacks as part of the climate forcing by using observed GHG changes for the past and calculated GHGs for the future, with calculated amounts based on carbon cycle and atmospheric chemistry models.

Climate forcings due to past changes in GHGs and surface albedo can be computed for the past 800 000 years using data from polar ice cores and ocean sediment cores. We use CO_2 [87] and CH_4 [88] data from Antarctic ice cores (figure 5*a*) to calculate an effective GHG forcing as follows:

$$\mathrm{Fe(GHGs)} = 1.12[\mathrm{Fa}(CO_2) + 1.4\mathrm{Fa}(CH_4)], \tag{5.2}$$

where Fa is the adjusted forcing, i.e. the planetary energy imbalance due to the GHG change after the stratospheric temperature has time to adjust to the gas change. Fe, the effective forcing, accounts for variable efficacies of different climate forcings [66]. Formulae for Fa of each gas are given by Hansen *et al.* [89]. The factor 1.4 converts the adjusted forcing of CH_4 to its effective forcing, Fe, which is greater than Fa mainly because of the effect of CH_4 on the tropospheric ozone and the stratospheric water vapour [66]. The factor 1.12 approximates the forcing by N_2O changes, which are not as well preserved in the ice cores but have a strong positive correlation with CO_2 and CH_4 changes [90]. The factor 1.12 is smaller than the 1.15 used by Hansen *et al.* [91], and is consistent with estimates of the N_2O forcing in the current Goddard Institute for Space Studies (GISS) radiation code and that of the Intergovernmental Panel on Climate Change (IPCC) [1,48]. Our LGM–Holocene GHG forcing (figure 5*c*) is approximately $3\,\mathrm{W\,m^{-2}}$, moderately larger than the $2.8\,\mathrm{W\,m^{-2}}$ estimated by IPCC [1,48] because of our larger effective CH_4 forcing.

Climate forcing due to surface albedo change is a function mainly of the sea level, which implicitly defines ice sheet size. Albedo change due to LGM–Holocene vegetation change, much of which is inherent with ice sheet area change, and albedo change due to coastline movement are lumped together with ice sheet area change in calculating the surface albedo climate forcing. An ice sheet forcing does not depend sensitively on the ice sheet shape or on how many ice sheets the ice volume is divided among and is nearly linear in sea-level change (see electronic supplementary material, figure S4, and [5]). For the sake of simplicity, we use the linear relation in Hansen *et al.* [5] and electronic supplementary material, figure S4; thus, $5\,\mathrm{W\,m^{-2}}$ between the LGM and ice-free conditions and $3.4\,\mathrm{W\,m^{-2}}$ between the LGM and Holocene. This scale factor was based on simulations with an early climate model [3,92]; comparable forcings are found in other models (e.g. see discussion in [93]), but results depend on cloud representations, assumed ice albedo and other factors; so the uncertainty is difficult to quantify. We subjectively estimate an uncertainty of approximately 20%.

Global temperature change obtained by multiplying the sum of the two climate forcings in figure 5*c* by a sensitivity of 3/4°C per $\mathrm{W\,m^{-2}}$ yields a remarkably good fit to 'observations' (figure 6), where the observed temperature is $2 \times \Delta T_{\mathrm{do}}$, with 2 being the scale factor required to yield the estimated 4.5°C LGM–Holocene surface temperature change. The close match is partly a result of the fact that sea-level and temperature data are derived from the same deep ocean record, but use of other sea-level reconstructions still yields a good fit between the calculated and observed temperature [5]. However, exactly the same match as in figure 6 is achieved with a fast-feedback sensitivity of 1°C per $\mathrm{W\,m^{-2}}$ if the LGM cooling is 6°C or with a sensitivity of 0.5°C per $\mathrm{W\,m^{-2}}$ if the LGM cooling is 3°C.

Accurate data defining LGM–Holocene warming would aid empirical evaluation of fast-feedback climate sensitivity. Remarkably, the range of recent estimates of LGM–Holocene warming, from approximately 3°C [94] to approximately 6°C [95], is about the same as at the time of the CLIMAP [96] project. Given today's much improved analytic capabilities, a new project to

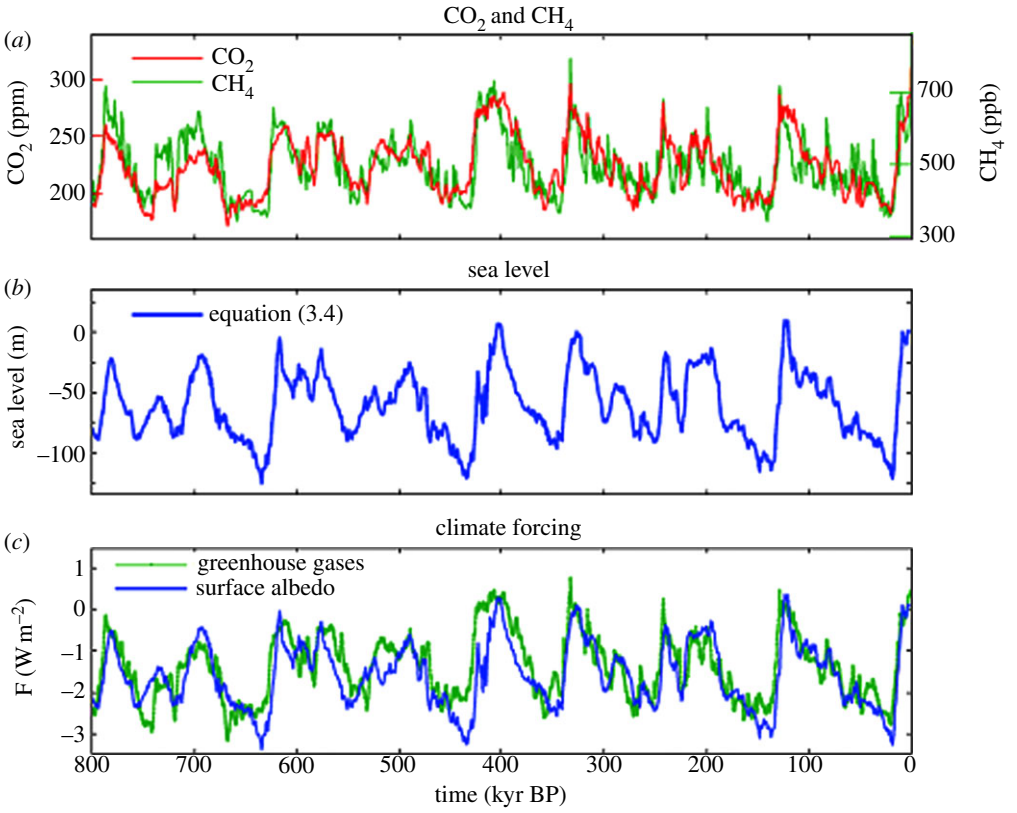

Figure 5. (*a*) CO_2 and CH_4 from ice cores; (*b*) sea level from equation (3.4) and (*c*) resulting climate forcings (see text).

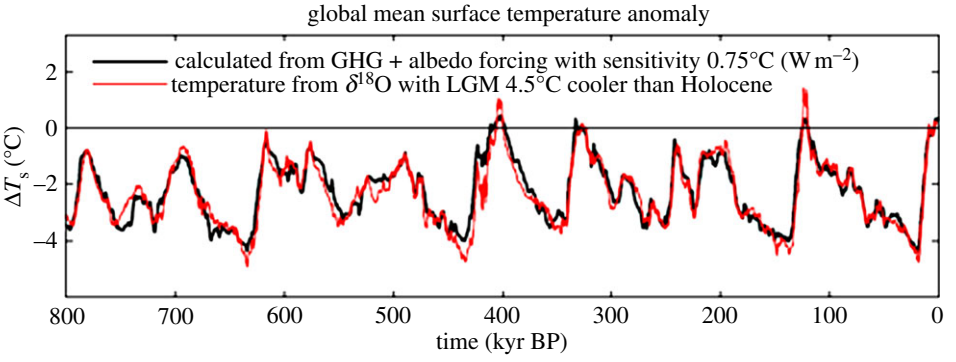

Figure 6. Calculated surface temperature for forcings of figure 5*c* with a climate sensitivity of 0.75°C per W m^{-2}, compared with $2 \times \Delta T_{do}$. Zero point is the Holocene (10 kyr) mean.

define LGM climate conditions, analogous to the Pliocene Research, Interpretation and Synoptic Mapping (PRISM) Pliocene data reconstruction [97,98] and Pliocene Model Intercomparison Project (PlioMIP) model intercomparisons [67,68], could be beneficial. In §7*b*, we suggest that a study of Eemian glacial–interglacial climate change could be even more definitive. Combined LGM, Eemian and Pliocene studies would address an issue raised at a recent workshop [99]: the need to evaluate how climate sensitivity varies as a function of the initial climate state. The calculations below were initiated after the workshop as another way to address that question.

(b) Fast-feedback sensitivity: state dependence

Climate sensitivity must be a strong function of the climate state. Simple climate models show that, when the Earth becomes cold enough for the ice cover to approach the tropics, the amplifying albedo feedback causes rapid ice growth to the Equator: 'snowball Earth' conditions [100]. Real-world complexity, including ocean dynamics, can mute this sharp bifurcation to a temporarily stable state [101], but snowball events have occurred several times in the Earth's history when the younger Sun was dimmer than today [102]. The Earth escaped snowball conditions owing to limited weathering in that state, which allowed volcanic CO_2 to accumulate in the atmosphere until there was enough CO_2 for the high sensitivity to cause rapid deglaciation [103].

Climate sensitivity at the other extreme, as the Earth becomes hotter, is also driven mainly by an H_2O feedback. As climate forcing and temperature increase, the amount of water vapour in the air increases and clouds may change. Increased water vapour makes the atmosphere more opaque in the infrared region that radiates the Earth's heat to space, causing the radiation to emerge from higher colder layers, thus reducing the energy emitted to space. This amplifying feedback has been known for centuries and was described remarkably well by Tyndall [104]. Ingersoll [105] discussed the role of water vapours in the 'runaway greenhouse effect' that caused the surface of Venus to eventually become so hot that carbon was 'baked' from the planet's crust, creating a hothouse climate with almost 100 bars of CO_2 in the air and a surface temperature of about 450°C, a stable state from which there is no escape. Arrival at this terminal state required passing through a 'moist greenhouse' state in which surface water evaporates, water vapour becomes a major constituent of the atmosphere and H_2O is dissociated in the upper atmosphere with the hydrogen slowly escaping to space [106]. That Venus had a primordial ocean, with most of the water subsequently lost to space, is confirmed by the present enrichment of deuterium over ordinary hydrogen by a factor of 100 [107], the heavier deuterium being less efficient in escaping gravity to space.

The physics that must be included to investigate the moist greenhouse is principally: (i) accurate radiation incorporating the spectral variation of gaseous absorption in both the solar radiation and thermal emission spectral regions, (ii) atmospheric dynamics and convection with no specifications favouring artificial atmospheric boundaries, such as between a troposphere and stratosphere, (iii) realistic water vapour physics, including its effect on atmospheric mass and surface pressure, and (iv) cloud properties that respond realistically to climate change. Conventional global climate models are inappropriate, as they contain too much other detail in the form of parametrizations or approximations that break down as climate conditions become extreme.

We use the simplified atmosphere–ocean model of Russell *et al.* [108], which solves the same fundamental equations (conservation of energy, momentum, mass and water substance, and the ideal gas law) as in more elaborate global models. Principal changes in the physics in the current version of the model are use of a step-mountain C-grid atmospheric vertical coordinate [109], addition of a drag in the grid-scale momentum equation in both atmosphere and ocean based on subgrid topography variations, and inclusion of realistic ocean tides based on exact positioning of the Moon and Sun. Radiation is the *k*-distribution method of Lacis & Oinas [110] with 25 *k*-values; the sensitivity of this specific radiation code is documented in detail by Hansen *et al.* [111]. Atmosphere and ocean dynamics are calculated on $3^\circ \times 4^\circ$ Arakawa C-grids. There are 24 atmospheric layers. In our present simulations, the ocean's depth is reduced to 100 m with five layers so as to achieve a rapid equilibrium response to forcings; this depth limitation reduces poleward ocean transport by more than half. Moist convection is based on a test of moist static stability as in Hansen *et al.* [92]. Two cloud types occur: moist convective clouds, when the atmosphere is moist statically unstable, and large-scale super-saturation, with cloud optical properties based on the amount of moisture removed to eliminate super-saturation, with scaling coefficients chosen to optimize the control run's fit with global observations [108,112]. To avoid long response times in extreme climates, today's ice sheets are assigned surface properties

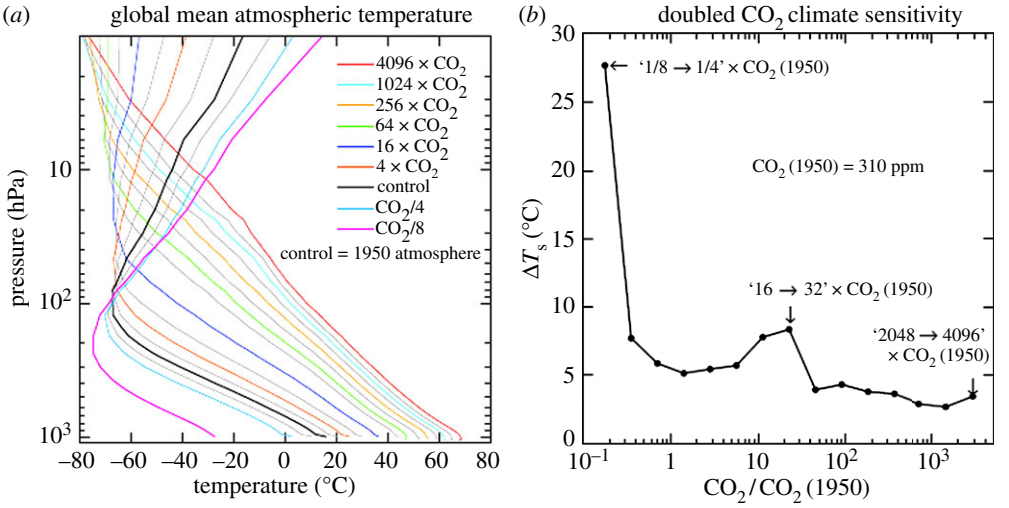

Figure 7. (*a*) The calculated global mean temperature for successive doublings of CO_2 (legend identifies every other case) and (*b*) the resulting climate sensitivity ($1 \times CO_2 = 310$ ppm).

of the tundra, thus allowing them to have a high albedo snow cover in cold climates but darker vegetation in warm climates. The model, the present experiments and more extensive experiments will be described in a forthcoming paper [112].

The equilibrium response of the control run (1950 atmospheric composition, CO_2 approx. 310 ppm) and runs with successive CO_2 doublings and halvings reveals that snowball Earth instability occurs just beyond three CO_2 halvings. Given that a CO_2 doubling or halving is equivalent to a 2% change in solar irradiance [66] and the estimate that solar irradiance was approximately 6% lower 600 Ma at the most recent snowball Earth occurrence [113], figure 7 implies that about 300 ppm CO_2 or less was sufficiently small to initiate glaciation at that time.

Climate sensitivity reaches large values at 8–32 × CO_2 (approx. 2500–10 000 ppm; figure 7*b*). High sensitivity is caused by increasing water vapour as the tropopause rises and diminishing low cloud cover, but the sensitivity decreases for still larger CO_2 as cloud optical thickness and planetary albedo increase, as shown by Russell *et al.* [112]. The high sensitivity for CO_2 less than $4 \times CO_2$ is due partly to the nature of the experiments (Greenland and Antarctic ice sheets being replaced by the tundra). High albedo snow cover on these continents largely disappears between $1 \times CO_2$ and $4 \times CO_2$, thus elevating the calculated fast-feedback sensitivity from approximately 4°C to approximately 5°C. In the real world, we would expect the Greenland and Antarctic ice sheets to be nearly eliminated and replaced by partially vegetated surfaces already at $2 \times CO_2$ (620 ppm) equilibrium climate. In other words, if the Greenland/Antarctic surface albedo change were identified as a slow feedback, rather than as a fast-feedback snow effect as it is in figure 7, the fast-feedback sensitivity at 1–4 × CO_2 would be approximately 4°C. Thus, the sensitivity approximately 8°C per CO_2 doubling in the range of 8–32 × CO_2 is a very large increase over sensitivity at smaller CO_2 amounts.

How confident are we in the modelled fast-feedback sensitivity (figure 7*b*)? We suspect that the modelled water vapour feedback may be moderately exaggerated, because the water vapour amount in the control run exceeds observed amounts. In addition, the area of sea ice in the control run exceeds observations, which may increase the modelled sensitivity in the 1–4 × CO_2 range. On the other hand, we probably underestimate the sensitivity at very high CO_2 amounts, because our model (such as most climate models) does not change the total atmospheric mass as the CO_2 amount varies. Mass change due to conceivable fossil fuel loading (up to say $16 \times CO_2$) is unlikely to have much effect, but sensitivity is probably underestimated at high CO_2 amounts owing to

self-broadening of CO_2 absorption lines. The increased atmospheric mass is also likely to alter the cloud feedback, which otherwise is a strongly diminishing feedback at very large CO_2 amounts. Atmospheric mass will be important after the Earth has lost its ocean and carbon is baked into the atmosphere. These issues are being examined by Russell *et al.* [112].

Earth today, with approximately 1.26 times 1950 CO_2, is far removed from the snowball state. Because of the increase in solar irradiance over the past 600 Myr and volcanic emissions, no feasible CO_2 amount could take the Earth back to snowball conditions. Similarly, a Venus-like baked-crust CO_2 hothouse is far distant because it cannot occur until the ocean escapes to space. We calculate an escape time of the order of 10^8–10^9 years even with the increased stratospheric water vapour and temperature at $16 \times CO_2$. Given the transient nature of a fossil fuel CO_2 injection, the continuing forcing required to achieve a terminal Venus-like baked-crust CO_2 hothouse must wait until the Sun's brightness has increased on the billion year time scale. However, the planet could become uninhabitable long before that.

The practical concern for humanity is the high climate sensitivity and the eventual climate response that may be reached if all fossil fuels are burned. Estimates of the carbon content of all fossil fuel reservoirs including unconventional fossil fuels such as tar sands, tar shale and various gas reservoirs that can be tapped with developing technology [114] imply that CO_2 conceivably could reach a level as high as 16 times the 1950 atmospheric amount. In that event, figure 7 suggests a global mean warming approaching 25°C, with much larger warming at high latitudes (see electronic supplementary material, figure S6). The result would be a planet on which humans could work and survive outdoors in the summer only in mountainous regions [115,116]—and there they would need to contend with the fact that a moist stratosphere would have destroyed the ozone layer [117].

6. Earth system sensitivity

GHG and surface albedo changes, which we treated as specified climate forcings in evaluating fast-feedback climate sensitivity, are actually slow climate feedbacks during orbit-instigated Pleistocene glacial–interglacial climate swings. Given that GHG and albedo feedbacks are both strong amplifying feedbacks, indeed accounting by themselves for most of the global Pleistocene climate variation, it is apparent that today's climate sensitivity on millennial time scales must be substantially larger than the fast-feedback sensitivity.

Climate sensitivity including slow feedbacks is described as 'Earth system sensitivity' [118–120]. There are alternative choices for the feedbacks included in Earth system sensitivity. Hansen & Sato [60] suggest adding slow feedbacks one by one, creating a series of increasingly comprehensive Earth system climate sensitivities; specifically, they successively move climate-driven changes in surface albedo, non-CO_2 GHGs and CO_2 into the feedback category, at which point the Earth system sensitivity is relevant to an external forcing such as changing solar irradiance or human-made forcings. At each level, in this series, the sensitivity is state dependent.

Our principal aim here is to use Cenozoic climate change to infer information on the all-important fast-feedback climate sensitivity, including its state dependence, via analysis of Earth system sensitivity. CO_2 is clearly the dominant forcing of the long-term Cenozoic cooling, in view of the abundant evidence that CO_2 reached levels of the order of 1000 ppm in the Early Cenozoic [9], as discussed in the Overview above. Thus, our approach is to examine Earth system sensitivity to CO_2 change by calculating the CO_2 history required to produce our reconstructed Cenozoic temperature history for alternative state-independent and state-dependent climate sensitivities. By comparing the resulting CO_2 histories with CO_2 proxy data, we thus assess the most realistic range for climate sensitivity.

Two principal uncertainties in this analysis are (i) global temperature at the EECO approximately 50 Myr BP and (ii) CO_2 amount at that time. We use EECO approximately 28°C (figure 4) as our standard case, but we repeat the analysis with EECO approximately 33°C (see electronic supplementary material, figure S3), thus allowing inference of how the conclusions change if knowledge of Eocene temperature changes.

Similarly, our graphs allow the inferred climate sensitivity to be adjusted if improved knowledge of CO_2 50 Myr BP indicates a value significantly different from approximately 1000 ppm.

To clarify our calculations, let us first assume that fast-feedback climate sensitivity is a constant (state-independent) 3°C for doubled CO_2 (0.75°C per W m^{-2}). It is then trivial to convert our global temperature for the Cenozoic (figure 4*a*) to the total climate forcing throughout the Cenozoic, which is shown in the electronic supplementary material, figure S4*a*, as are results of subsequent steps. Next, we subtract the solar forcing, a linear increase of 1 W m^{-2} over the Cenozoic era due to the Sun's 0.4% irradiance increase [121], and the surface albedo forcing due to changing ice sheet size, which we take as linear at 5 W m^{-2} for the 180 m sea-level change from 35 Myr BP to the LGM. These top-of-the-atmosphere and surface forcings are moderate in size, compared with the total forcing over the Cenozoic, and partially offsetting, as shown in the electronic supplementary material, figure S4*b*. The residual forcing, which has a maximum of approximately 17 W m^{-2} just prior to 50 Myr BP, is the atmospheric forcing due to GHGs. Non-CO_2 GHGs contribute 25% of the total GHG forcing in the period of ice core measurements. Atmospheric chemistry simulations [122] reveal continued growth of non-CO_2 gases (N_2O, CH_4 and tropospheric O_3) in warmer climates, at only a slightly lower rate (1.7–2.3 W m^{-2} for 4 × CO_2, which itself is approx. 8 W m^{-2}). Thus, we take the CO_2 forcing as 75% of the GHG forcing throughout the Cenozoic in our standard case, but we also consider the extreme case in which non-CO_2 gases are fixed and thus contribute no climate forcing.

A CO_2 forcing is readily converted to the CO_2 amount; we use the equation in table 1 of Hansen *et al.* [89]. The resulting Cenozoic CO_2 history required to yield the global surface temperature of figure 4*a* is shown in figure 8*a* for state-independent climate sensitivity with non-CO_2 GHGs providing 25% of the GHG climate forcing. The peak CO_2 in this case is approximately 2000 ppm. If non-CO_2 GHGs provide less than 25% of the total GHG forcing, then the inferred CO_2 amount would be even greater. Results for alternative sensitivities, as in figure 8*b*, are calculated for a temporal resolution of 0.5 Myr to smooth out glacial–interglacial CO_2 oscillations, as our interest here is in CO_2 as a climate forcing.

We focus on the CO_2 amount 50 Myr BP averaged over a few million years in assessing the realism of our inferred CO_2 histories, because CO_2 variations in the Cenozoic remain very uncertain despite the success of Beerling & Royer [9] in eliminating the most extreme outliers. Beerling & Royer [9] find a best-fit CO_2 at 50 Myr BP of about 1000 ppm—see their figure 1, which also indicates that CO_2 at 50 Myr BP was almost certainly in the range of 750–1500 ppm, even though it is impossible to provide a rigorous confidence interval.

We conclude that the average fast-feedback climate sensitivity during the Cenozoic is larger than the canonical 3°C for 2 × CO_2 (0.75°C per W m^{-2}) that has long been the central estimate for current climate. An average 4°C for 2 × CO_2 (1°C per W m^{-2}) provides a good fit to the target 1000 ppm CO_2, but the sensitivity must be still higher if non-CO_2 GHG forcings amplify the CO_2 by less than one-third, i.e. provide less than 25% of the total GHG forcing.

(a) State-dependent climate sensitivity

More realistic assessment should account for the state dependence of climate sensitivity. Thus, we make the same calculations for the state-dependent climate sensitivity of the Russell climate model, i.e. we use the fast-feedback climate sensitivity of figure 7*b*. In addition, for the purpose of assessing how the results depend upon climate sensitivity, we consider a second case in which we reduce the Russell sensitivity of figure 7*b* by the factor two-thirds.

The estimated 1000 ppm of CO_2 at 50 Myr BP falls between the Russell sensitivity and two-thirds of the Russell sensitivity, though closer to the full Russell sensitivity. If the non-CO_2 GHG forcing is less than one-third of the CO_2 forcing, the result is even closer to the full Russell sensitivity. With these comparisons at 50 Myr BP in mind, we can use figure 9 to infer the likely CO_2 amount at other times. The End-Eocene transition began at about 500 ppm and fell to about 400 ppm. The Mid-Miocene warmth, which peaked at about 15 Myr BP, required a CO_2 increase

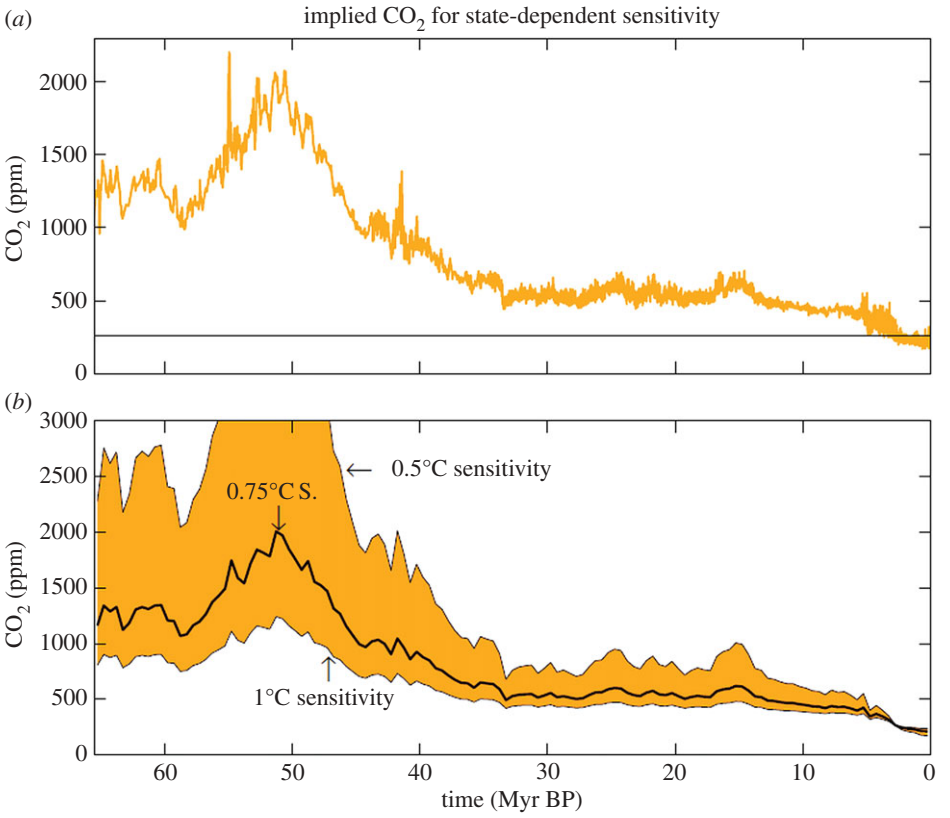

Figure 8. (*a*) CO_2 amount required to yield a global temperature of figure 4*a* if fast-feedback climate sensitivity is 0.75°C per W m^{-2} and non-CO_2 GHGs contribute 25% of the GHG forcing. (*b*) Same as in (*a*), but with temporal resolution 0.5 Myr and for three choices of fast-feedback sensitivity; the CO_2 peak exceeds 5000 ppm in the case of 0.5°C sensitivity. The horizontal line is the Early–Mid-Holocene 260 ppm CO_2 level.

of only a few tens of ppm with the Russell sensitivity, but closer to 100 ppm if the true sensitivity is only two-thirds of the Russell sensitivity. The higher (full Russell) sensitivity requires much less CO_2 change to produce the Mid-Miocene warming for two reasons: (i) the greater temperature change for a specified forcing and (ii) the smaller CO_2 change required to yield a given forcing from the lesser CO_2 level of the higher sensitivity case. The average CO_2 amount in the Early Pliocene is about 300 ppm for the Russell sensitivity, but could reach a few tens of ppm higher if the true sensitivity is closer to two-thirds of the Russell sensitivity.

(b) Comparison with van de Wal *et al.* model

van de Wal *et al.* [123] used the same Zachos *et al.* [4] $\delta^{18}O$ data to drive an inverse model calculation, including an ice sheet model to separate ice volume and temperature, thus inferring CO_2 over the past 20 Myr. They find an MMCO CO_2 approximately 450 ppm, which falls between the Russell and two-thirds Russell sensitivities (figure 9). The van de Wal *et al.* [123] model has a 30°C change in Northern Hemisphere temperature (their model is hemispheric) between the MMCO and average Pleistocene conditions driven by a CO_2 decline from approximately 450 ppm to approximately 250 ppm, which is a forcing of approximately 3.5 W m^{-2}. Thus, the implied (Northern Hemisphere) Earth system sensitivity is an implausible approximately 35°C for a 4 W m^{-2} CO_2 forcing. The large temperature change may be required to produce substantial sea-level change in their ice sheet model, which we suggested above is unrealistically unresponsive

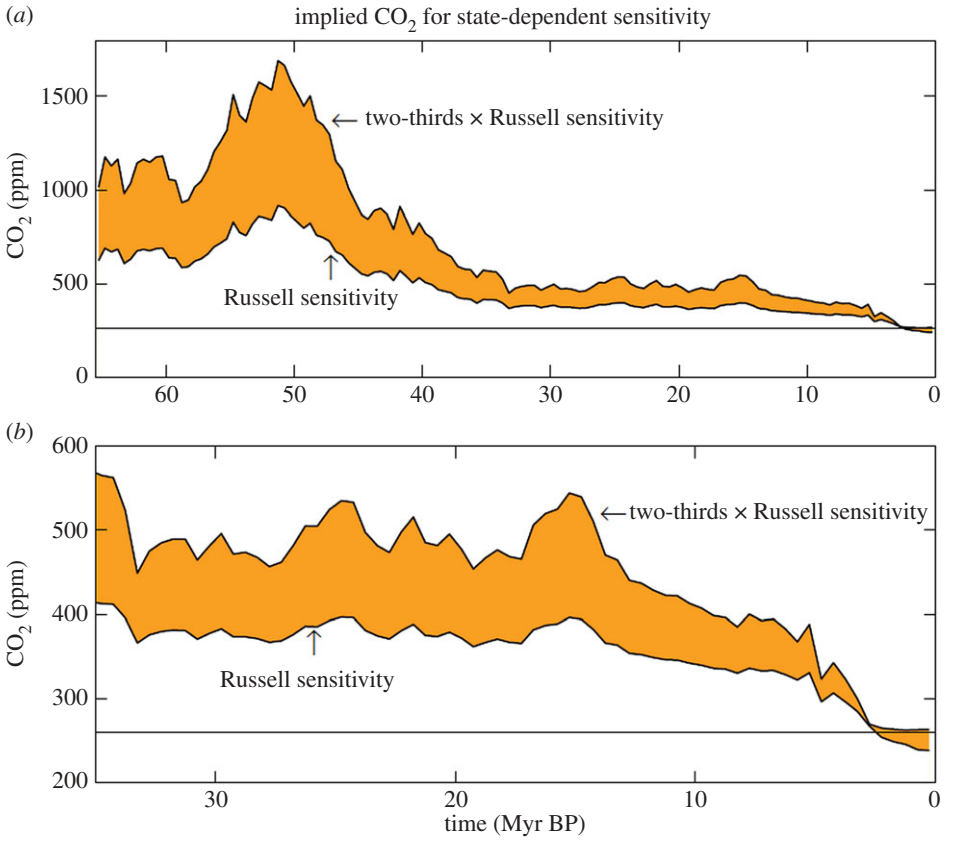

Figure 9. (*a*) CO_2 amount required to yield the global temperature history of figure 4*a* if fast-feedback climate sensitivity is that calculated with the Russell model, i.e. the sensitivity shown in figure 7*b*, and two-thirds of that sensitivity. These results assume that non-CO_2 GHGs provide 25% of the GHG climate forcing. (*b*) Vertical expansion for the past 35 Myr.

to climate change. However, they assign most of the temperature change to slow feedbacks, thus inferring a fast-feedback sensitivity of only about 3°C per CO_2 doubling.

(c) Inferences from the Palaeocene–Eocene Thermal Maximum and Early Cenozoic climate

Finally, we use the largest and best documented of the hyperthermals, the PETM, to test the reasonableness of the Russell state-dependent climate sensitivity. Global warming in the PETM is reasonably well defined at 5–6°C and the plausible range for carbon mass input is approximately 4000–7000 Pg C [14]. Given that the PETM carbon injection occurred over a period of a few millennia, carbon cycle models suggest that about one-third of the carbon would be airborne as CO_2 following complete injection [21]. With a conversion factor of 1 ppm $CO_2 \sim 2.12$ Gt C, the 4000–7000 Gt C source thus yields approximately 630–1100 ppm CO_2. We can use figure 10, obtained via the same calculations as described above, to see how much CO_2 is required to yield a 5°C warming. The Russell sensitivity requires approximately 800 ppm CO_2 for a 5°C warming, whereas two-thirds of the Russell sensitivity requires approximately 2100 ppm CO_2. Given the uncertainty in the airborne fraction of CO_2 and possible non-CO_2 gases, we cannot rule out the two-thirds Russell sensitivity, but the full Russell sensitivity fits plausible PETM carbon sources much better, especially if the PETM warming is actually somewhat more than 5°C (see figure 10 for quantitative implications).

This analysis is for Earth system sensitivity with CO_2 as the forcing, as is appropriate for the PETM because any carbon injected as CH_4 would be rapidly oxidized to CO_2. Feedbacks

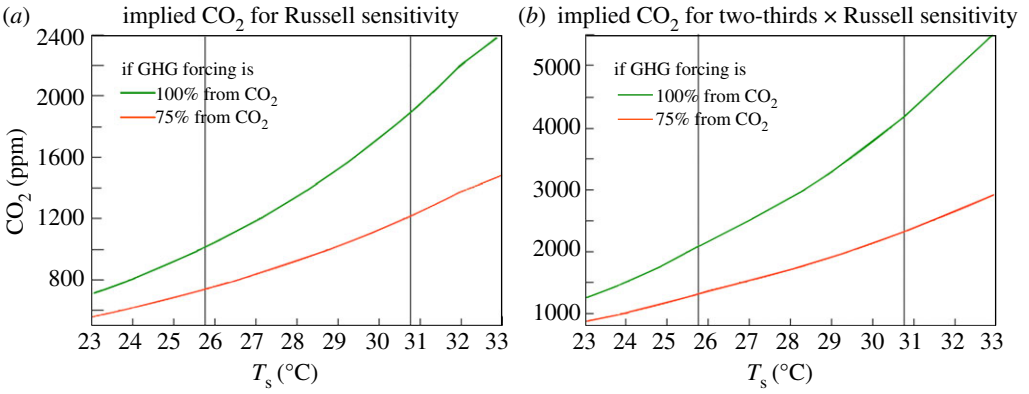

Figure 10. Atmospheric CO_2 amount (*y*-axis) required to yield a given global temperature (*x*-axis) at the time of the PETM for (*a*) the Russell climate sensitivity and (*b*) two-thirds of the Russell sensitivity. The CO_2 increment required to yield a given PETM warming above the pre-PETM temperature (25.7°C) is obtained by subtracting the CO_2 amount at the desired T_s from the CO_2 at $T_s = 25.7$°C. The vertical line is for the case of 5°C PETM warming. The orange lines show the required CO_2 if the CO_2 increase is accompanied by a non-CO_2 GHG feedback that provides 25% of the total GHG forcing.

in the PETM do not include large ice sheets, but non-CO_2 GHGs are an unmeasured feedback. If a warming climate increases the amount of N_2O and CH_4 in the air, the required carbon source for a given global warming is reduced, because the amount of carbon in airborne CH_4 is negligible. Any non-CO_2 GHG feedback increases the CO_2-forced Earth system sensitivity, potentially by a large amount (figure 10). The CO_2-forced Earth sensitivity is the most relevant climate sensitivity, not only for the PETM but for human-made forcings. Although present enhanced amounts of airborne CH_4 and N_2O are mostly a climate forcing, i.e. their increases above the pre-industrial level are mainly a consequence of human-made sources, they also include a GHG feedback. Climate sensitivity including this GHG feedback is the most relevant sensitivity for humanity as the CO_2 forcing continues to grow.

If the EECO global temperature exceeded 28°C, as suggested by multi-proxy data taken at face value (see above), climate sensitivity implied by the EECO warmth and the PETM warming is close to the full Russell climate sensitivity (see electronic supplementary material, figures S7–S9). We conclude that the existing data favour a climate sensitivity of at least two-thirds of the Russell sensitivity, and probably closer to the full Russell sensitivity. That lower limit is just over 3°C for $2 \times CO_2$ for the range of climate states of immediate relevance to humanity (figure 7*b*).

7. Summary discussion

Covariation of climate, sea level and atmospheric CO_2 through the Cenozoic era is a rich source of information that can advise us about the sensitivity of climate and ice sheets to forcings, including human-made forcings. Our approach is to estimate Cenozoic sea level and temperature from empirical data, with transparent assumptions and minimal modelling. Our data are available in the electronic supplementary material, allowing comparison with other data and model results.

(a) Sea-level sensitivity

Hansen [49,50] argues that real ice sheets are more responsive to warming than in most ice sheet models, which suggests that large ice sheets are relatively stable. The model of Pollard & DeConto [124], for example, requires three to four times the pre-industrial CO_2 amount to melt the Antarctic ice sheet. This stability is, in part, a result of hysteresis: as the Earth warms, the ice sheet size as a function of temperature does not return on the same path that it followed as temperature fell and the ice sheet grew. We do not question the reality of mechanisms that cause ice sheet

hysteresis, but we suspect they are exaggerated in models. Thus, as an extreme alternative that can be compared with ice sheet models and real-world data, we assume that hysteresis effects are negligible in our approximation for sea level as a function of temperature.

Ice sheets in question are those on Greenland and Antarctica, ice sheets that could shrink with future warming. Despite the stability of those ice sheets in the Holocene, there is evidence that sea level was much more variable during the Eemian, when we estimate the peak global temperature was only +1.0°C warmer than in the first decade of the twenty-first century. Rohling *et al.* [52] estimate an average rate of Eemian sea-level change of 1.4 m per century, and several studies noted above suggest that the Eemian sea level reached heights of +4–6 m or more relative to today.

The MMCO provides one test of hysteresis. Our sea-level approximation (figure 2) suggests that the Antarctic ice sheet nearly disappeared at that time. John *et al.* [125] provide support for that interpretation, as well as evidence of numerous rises and falls of sea level by 20–30 m during the Miocene. These variations are even larger than those we find (figure 2), but the resolution of the $\delta^{18}O$ data we use is not adequate to provide the full amplitude of variations during that period (electronic supplementary material, figure S1).

The Mid-Pliocene is a more important test of ice sheet variability. We find sea-level fluctuations of at least 20–40 m, much greater than in ice sheet models (figure 2), with global temperature variations of only a few degrees. Independent analyses designed to separate ice volume and temperature change, such as Dwyer & Chandler [64], find sea-level maxima and variability comparable to our estimates. Altogether, the empirical data support a high sensitivity of the sea level to global temperature change, and they provide strong evidence against the seeming lethargy and large hysteresis effects that occur in at least some ice sheet models.

(b) Fast-feedback climate sensitivity

Estimates of climate sensitivity cover a wide range that has existed for decades [1,48,99]. That range measures our ignorance; it does not mean that climate response from a specified state is stochastic with such inherent uncertainty. God (Nature) plays dice, but not for such large amounts. Indeed, one implication of the tight fit of calculated and measured temperature change of the past 800 000 years (figure 6) is that there is a single well-defined, but unknown, fast-feedback global climate sensitivity for that range of climate, despite large regional climate variations and ocean dynamical effects [31].

Improved empirical data can define climate sensitivity much more precisely, provided that climate-induced aerosol changes are included in the category of fast feedbacks (human-made aerosol changes are a climate forcing). Empirical assessment of fast-feedback climate sensitivity is obtained by comparing two quasi-equilibrium climate states for which boundary condition climate forcings (which may be slow feedbacks) are known. Aerosol changes between those climate states are appropriately included as a fast feedback, not only because aerosols respond rapidly to changing climate but also because there are multiple aerosol compositions, they have complex radiative properties and they affect clouds in several ways, thus making accurate knowledge of their glacial–interglacial changes inaccessible.

The temporal variation of the GHG plus surface albedo climate forcing closely mimics the temporal variation of either the deep ocean temperature (figure 6) or Antarctic temperature [5,31] for the entire 800 000 years of polar ice core data. However, the temperature change must be converted to the global mean to allow inference of climate sensitivity. The required scale factor is commonly extracted from an estimated LGM–Holocene global temperature change, which, however, is very uncertain, with estimates ranging from approximately 3°C to approximately 6°C. Thus, for example, the climate sensitivity (1.7–2.6°C for $2 \times CO_2$) estimated by Schmittner *et al.* [94] is due largely to their assumed approximately 3°C cooling in the LGM, and in lesser part to the fact that they defined some aerosol changes (dust) to be a climate forcing.

Climate sensitivity extracted from Pleistocene climate change is thus inherently partly subjective as it depends on how much weight is given to mutually inconsistent estimates of glacial-to-interglacial global temperature change. Our initial assessment is a fast-feedback

sensitivity of $3 \pm 1^{\circ}$C for $2 \times CO_2$, corresponding to an LGM cooling of 4.5°C, similar to the 2.2–4.8°C estimate of PALAEOSENS [99]. This sensitivity is higher than estimated by Schmittner *et al.* [94], partly because they included natural aerosol changes as a forcing. In addition, we note that their proxies for LGM sea surface cooling exclude planktic foraminifera data, which suggest larger cooling [126], and, as noted by Schneider von Deimling *et al.* [95], regions that are not sampled tend to be ones where the largest cooling is expected. It should be possible to gain consensus on a narrower range for climate sensitivity via a community project for the LGM analogous to PRISM Pliocene data reconstruction [97,98] and PlioMIP model intercomparisons [67,68].

However, we suggest that an even more fruitful approach would be a focused effort to define the glacial-to-interglacial climate change of the Eemian period (MIS-5e). The Eemian avoids the possibility of significant human-made effects, which may be a factor in the Holocene. Ruddiman [127] suggests that deforestation and agricultural activities affected CO_2 and CH_4 in the Holocene, and Hansen *et al.* [91] argue that human-made aerosols were probably important. Given the level of Eemian warmth, approximately +1.8°C relative to 1880–1920, with a climate forcing similar to that for LGM–Holocene (figure 5), we conclude that this relatively clean empirical assessment yields a fast-feedback climate sensitivity in the upper part of the range suggested by the LGM–Holocene climate change, i.e. a sensitivity of 3–4°C for $2 \times CO_2$. Detailed study is especially warranted because Eemian warmth is anticipated to recur in the near term.

(c) Earth system sensitivity

We have shown that global temperature change over the Cenozoic era is consistent with CO_2 change being the climate forcing that drove the long-term climate change. Proxy CO_2 measurements are so variable and uncertain that we only rely on the conclusion that the CO_2 amount was of the order of 1000 ppm during peak Early Eocene warmth. That conclusion, in conjunction with a climate model incorporating only the most fundamental processes, constrains average fast-feedback climate sensitivity to be in the upper part of the sensitivity range that is normally quoted [1,48,99], i.e. the sensitivity is greater than 3°C for $2 \times CO_2$. Strictly this Cenozoic evaluation refers to the average fast-feedback sensitivity for the range of climates from ice ages to peak Cenozoic warmth and to the situation at the time of the PETM. However, it would be difficult to achieve that high average sensitivity if the current fast-feedback sensitivity were not at least in the upper half of the range of $3 \pm 1^{\circ}$C for $2 \times CO_2$.

This climate sensitivity evaluation has implications for the atmospheric CO_2 amount throughout the Cenozoic era, which can be checked as improved proxy CO_2 measurements become available. The CO_2 amount was only approximately 450–500 ppm 34 Myr BP when large-scale glaciation first occurred on Antarctica. Perhaps more important, the amount of CO_2 required to melt most of Antarctica in the MMCO was only approximately 450–500 ppm, conceivably only about 400 ppm. These CO_2 amounts are smaller than suggested by ice sheet/climate models, providing further indication that the ice sheet models are excessively lethargic, i.e. resistant to climate change. The CO_2 amount in the earliest Pliocene, averaged over astronomical cycles, was apparently only about 300 ppm, and decreased further during the Pliocene.

(d) Runaway greenhouse

Our climate simulations, using a simplified three-dimensional climate model to solve the fundamental equations for conservation of water, atmospheric mass, energy, momentum and the ideal gas law, but stripped to basic radiative, convective and dynamical processes, finds upturns in climate sensitivity at the same forcings as found with a more complex global climate model [66]. At forcings beyond these points the complex model 'crashed', as have other climate models (discussed by Lunt *et al.* [83]). The upturn at the 10–20 $W\,m^{-2}$ negative forcing has a simple physical explanation: it is the snowball Earth instability. Model crashes for large positive forcings are sometimes described as a runaway greenhouse, but they probably are caused by one

of the many parametrizations in complex global models going outside its range of validity, not by a runaway greenhouse effect.

The runaway greenhouse effect has several meanings ranging from, at the low end, global warming sufficient to induce out-of-control amplifying feedbacks, such as ice sheet disintegration and melting of methane hydrates, to, at the high end, a Venus-like hothouse with crustal carbon baked into the atmosphere and a surface temperature of several hundred degrees, a climate state from which there is no escape. Between these extremes is the moist greenhouse, which occurs if the climate forcing is large enough to make H_2O a major atmospheric constituent [106]. In principle, an extreme moist greenhouse might cause an instability with water vapour preventing radiation to space of all absorbed solar energy, resulting in very high surface temperature and evaporation of the ocean [105]. However, the availability of non-radiative means for vertical transport of energy, including small-scale convection and large-scale atmospheric motions, must be accounted for, as is done in our atmospheric general circulation model. Our simulations indicate that no plausible human-made GHG forcing can cause an instability and runaway greenhouse effect as defined by Ingersoll [105], in agreement with the theoretical analyses of Goldblatt & Watson [128].

On the other hand, conceivable levels of human-made climate forcing could yield the low-end runaway greenhouse. A forcing of 12–16 W m^{-2}, which would require CO_2 to increase by a factor of 8–16 times, if the forcing were due only to CO_2 change, would raise the global mean temperature by 16–24°C with much larger polar warming. Surely that would melt all the ice on the planet, and probably thaw methane hydrates and scorch carbon from global peat deposits and tropical forests. This forcing would not produce the extreme Venus-like baked-crust greenhouse state, which cannot be reached until the ocean is lost to space. A warming of 16–24°C produces a moderately moist greenhouse, with water vapour increasing to about 1% of the atmosphere's mass, thus increasing the rate of hydrogen escape to space. However, if the forcing is by fossil fuel CO_2, the weathering process would remove the excess atmospheric CO_2 on a time scale of 10^4–10^5 years, well before the ocean is significantly depleted. Baked-crust hothouse conditions on the Earth require a large long-term forcing that is unlikely to occur until the sun brightens by a few tens of per cent, which will take a few billion years [121].

(e) Global habitability

Burning all fossil fuels would produce a different, practically uninhabitable, planet. Let us first consider a 12 W m^{-2} greenhouse forcing, which we simulated with 8 × CO_2. If non-CO_2 GHGs such as N_2O and CH_4 increase with global warming at the same rate as in the palaeoclimate record and atmospheric chemistry simulations [122], these other gases provide approximately 25% of the greenhouse forcing. The remaining 9 W m^{-2} forcing requires approximately 4.8 × CO_2, corresponding to fossil fuel emissions as much as approximately 10,000 Gt C for a conservative assumption of a CO_2 airborne fraction averaging one-third over the 1000 years following a peak emission [21,129].

Our calculated global warming in this case is 16°C, with warming at the poles approximately 30°C. Calculated warming over land areas averages approximately 20°C. Such temperatures would eliminate grain production in almost all agricultural regions in the world [130]. Increased stratospheric water vapour would diminish the stratospheric ozone layer [131].

More ominously, global warming of that magnitude would make most of the planet uninhabitable by humans [132,133]. The human body generates about 100 W of metabolic heat that must be carried away to maintain a core body temperature near 37°C, which implies that sustained wet bulb temperatures above 35°C can result in lethal hyperthermia [132,134]. Today, the summer temperature varies widely over the Earth's surface, but wet bulb temperature is more narrowly confined by the effect of humidity, with the most common value of approximately 26–27°C and the highest approximately of 31°C. A warming of 10–12°C would put most of today's world population in regions with wet a bulb temperature above 35°C [132]. Given the 20°C warming we find with 4.8 × CO_2, it is clear that such a climate forcing would produce

intolerable climatic conditions even if the true climate sensitivity is significantly less than the Russell sensitivity, or, if the Russell sensitivity is accurate, the CO_2 amount required to produce intolerable conditions for humans is less than $4.8 \times CO_2$. Note also that increased heat stress due to warming of the past few decades is already enough to affect health and workplace productivity at low latitudes, where the impact falls most heavily on low- and middle-income countries [135].

The Earth was 10–12°C warmer than today in the Early Eocene and at the peak of the PETM (figure 4). How did mammals survive that warmth? Some mammals have higher internal temperatures than humans and there is evidence of evolution of surface-area-to-mass ratio to aid heat dissipation, for example transient dwarfing of mammals [136] and even soil fauna [137] during the PETM warming. However, human-made warming will occur in a few centuries, as opposed to several millennia in the PETM, thus providing little opportunity for evolutionary dwarfism to alleviate impacts of global warming. We conclude that the large climate change from burning all fossil fuels would threaten the biological health and survival of humanity, making policies that rely substantially on adaptation inadequate.

Let us now verify that our assumed fossil fuel climate forcing of $9\,W\,m^{-2}$ is feasible. If we assume that fossil fuel emissions increase by 3% per year, typical of the past decade and of the entire period since 1950, cumulative fossil fuel emissions will reach 10 000 Gt C in 118 years. However, with such large rapidly growing emissions the assumed 33% CO_2 airborne fraction is surely too small. The airborne fraction, observed to have been 55% since 1950 [1], should increase because of well-known nonlinearity in ocean chemistry and saturation of carbon sinks, implying that the airborne fraction probably will be closer to two-thirds rather than one-third, at least for a century or more. Thus, the fossil fuel source required to yield a $9\,W\,m^{-2}$ forcing may be closer to 5000 Gt C, rather than 10 000 Gt C.

Are there sufficient fossil fuel reserves to yield 5000–10 000 Gt C? Recent updates of potential reserves [114], including unconventional fossil fuels (such as tar sands, tar shale and hydrofracking-derived shale gas) in addition to conventional oil, gas and coal, suggest that $5 \times CO_2$ (1400 ppm) is indeed feasible. For instance, using the emission factor for coal from IPCC [48], coal resources given by the Global Energy Assessment [114] amount to 7300–11 000 Gt C. Similarly, using emission factors from IPCC [48], total recoverable fossil energy reserves and resources estimated by GEA [114] are approximately 15 000 Gt C. This does not include large 'additional occurrences' listed in ch. 7 of GEA [114]. Thus, for a multi-centennial CO_2 airborne fraction between one-third and two-thirds, as discussed above, there are more than enough available fossil fuels to cause a forcing of $9\,W\,m^{-2}$ sustained for centuries.

Most of the remaining fossil fuel carbon is in coal and unconventional oil and gas. Thus, it seems, humanity stands at a fork in the road. As conventional oil and gas are depleted, will we move to carbon-free energy and efficiency—or to unconventional fossil fuels and coal? If fossil fuels were made to pay their costs to society, costs of pollution and climate change, carbon-free alternatives might supplant fossil fuels over a period of decades. However, if governments force the public to bear the external costs and even subsidize fossil fuels, carbon emissions are likely to continue to grow, with deleterious consequences for young people and future generations.

It seems implausible that humanity will not alter its energy course as consequences of burning all fossil fuels become clearer. Yet strong evidence about the dangers of human-made climate change have so far had little effect. Whether governments continue to be so foolhardy as to allow or encourage development of all fossil fuels may determine the fate of humanity.

Acknowledgements. We thank James Zachos for the deep ocean oxygen isotope data; Chris Brierly, Mark Chandler, Bas de Boer, Alexey Fedorov, Chris Hatfield, Dorothy Peteet, David Rind, Robert Rohde and Cynthia Rosenzweig for helpful information; Andy Ridgwell for useful editorial suggestions and patience; Eelco Rohling for ably organizing the palaeoclimate workshop that spurred the writing of this paper; Gerry Lenfest (Lenfest Foundation), ClimateWorks, Lee Wasserman (Rockefeller Family Foundation), Stephen Toben (Flora Family Foundation) and NASA program managers Jack Kaye and David Considine for research support.

References

1. Intergovernmental Panel on Climate Change. 2007 *Climate change 2007: the physical science basis* (eds S Solomon *et al.*). Cambridge, UK: Cambridge University Press.
2. Hansen J, Sato M, Kharecha P, von Schuckmann K. 2011 Earth's energy imbalance and implications. *Atmos. Chem. Phys.* **11**, 13 421–13 449. (doi:10.5194/acp-11-13421-2011)
3. Hansen J, Lacis A, Rind D, Russell G, Stone P, Fung I, Ruedy R, Lerner J. 1984 Climate sensitivity: analysis of feedback mechanisms. In *Climate processes and climate sensitivity* (eds JE Hansen, T Takahashi), pp. 130–163. AGU Geophysical Monograph 29, Maurice Ewing vol. 5. Washington, DC: American Geophysical Union.
4. Zachos JC, Dickens GR, Zeebe RE. 2008 An Early Cenozoic perspective on greenhouse warming and carbon-cycle dynamics. *Nature* **451**, 279–283. (doi:10.1038/nature06588)
5. Hansen J *et al.* 2008 Target atmospheric CO_2: where should humanity aim? *Open Atmos. Sci. J.* **2**, 217–231. (doi:10.2174/1874282300802010217)
6. Zachos J, Pagani M, Sloan L, Thomas E, Billups K. 2001 Trends, rhythms, and aberrations in global climate 65 Ma to present. *Science* **292**, 686–693. (doi:10.1126/science.1059412)
7. Gasson E, Siddall M, Lunt DJ, Rackham OJL, Lear CH, Pollard D. 2012 Exploring uncertainties in the relationship between temperature, ice volume, and sea level over the past 50 million years. *Rev. Geophys.* **50**, RG1005. (doi:10.1029/2011RG000358)
8. Kent DV, Muttoni G. 2008 Equatorial convergence of India and Early Cenozoic climate trends. *Proc. Natl Acad. Sci. USA* **105**, 16 065–16 070. (doi:10.1073/pnas.0805382105)
9. Beerling DJ, Royer DL. 2011 Convergent Cenozoic CO_2 history. *Nat. Geosci.* **4**, 418–420. (doi:10.1038/ngeo1186)
10. Edmond JM, Huh Y. 2003 Non-steady state carbonate recycling and implications for the evolution of atmospheric P_{CO_2}. *Earth Planet. Sci. Lett.* **216**, 125–139. (doi:10.1016/S0012-821X(03)00510-7)
11. Petit JR *et al.* 1999 Climate and atmospheric history of the past 420 000 years from the Vostok ice core, Antarctica. *Nature* **399**, 429–436. (doi:10.1038/20859)
12. Kennett JP, Stott LD. 1991 Abrupt deep-sea warming, paleoceanographic changes and benthic extinctions at the end of the Paleocene. *Nature* **353**, 225–229. (doi:10.1038/353225a0)
13. Bohaty SM, Zachos JC, Florindo F, Delaney ML. 2009 Coupled greenhouse warming and deep-sea acidification in the middle Eocene. *Paleoceanography* **24**, PA2207. (doi:10.1029/2008PA001676)
14. Dunkley Jones T, Ridgwell A, Lunt DJ, Maslin MA, Schmidt DN, Valdes PJ. 2010 A Palaeogene perspective on climate sensitivity and methane hydrate instability. *Phil. Trans. R. Soc. A* **368**, 2395–2415. (doi:10.1098/rsta.2010.0053)
15. Dickens GR, O'Neil JR, Rea DK, Owen RM. 1995 Dissociation of oceanic methane hydrate as a cause of the carbon isotope excursion at the end of the Paleocene. *Paleoceanography* **10**, 965–971. (doi:10.1029/95PA02087)
16. DeConto RM, Galeotti S, Pagani M, Tracy D, Schaefer K, Zhang T, Pollard D, Beerling DJ. 2012 Past extreme warming events linked to massive carbon release from thawing permafrost. *Nature* **484**, 87–91. (doi:10.1038/nature10929)
17. Lourens LJ, Sluijs A, Kroon D, Zachos JC, Thomas E, Rohl U, Bowles J, Raffi I. 2005 Astronomical pacing of Late Palaeocene to Early Eocene global warming events. *Nature* **435**, 1083–1087. (doi:10.1038/nature03814)
18. Lunt DJ, Ridgwell A, Sluijs A, Zachos J, Hunter S, Haywood A. 2011 A model for orbital pacing of methane hydrate destabilization during the Palaeogene. *Nat. Geosci.* **4**, 775–778. (doi:10.1038/ngeo1266)
19. Sluijs A *et al.* 2007 Environmental precursors to rapid light carbon injection at the Palaeocene/Eocene boundary. *Nature* **450**, 1218–1221. (doi:10.1038/nature06400)
20. Lunt DJ, Valdes PJ, Dunkley Jones T, Ridgwell A, Haywood AM, Schmidt DN, Marsh R, Maslin M. 2010 CO_2-driven ocean circulation changes as an amplifier of Paleocene–Eocene thermal maximum hydrate destabilization. *Geology* **38**, 875–878. (doi:10.1130/G31184.1)
21. Archer D. 2005 Fate of fossil fuel CO_2 in geologic time. *J. Geophys. Res.* **110**, C09505. (doi:10.1029/2004JC002625)
22. Thomas DJ, Zachos JC, Bralower TJ, Thomas E, Bohaty S. 2002 Warming the fuel for the fire: evidence for the thermal dissociation of methane hydrate during the Paleocene–Eocene thermal maximum. *Geology* **30**, 1067–1070. (doi:10.1130/0091-7613(2002)030<1067:WTFFTF>2.0.CO;2)

23. Ivanov M, Bohme M. 2011 Snakes from Greisbeckerzell (Langhian, Early Badenian), North Alpine Foreland Basin (Germany), with Comments on the Evolution of Snake Faunas in Central Europe during the Miocene Climatic Optimum. *Geodiversitas* **33**, 411–449. (doi:10.5252/g2011n3a2)
24. Feakins SJ, Warny S, Lee JE. 2012 Hydrologic cycling over Antarctica during the middle Miocene warming. *Nat. Geosci.* **5**, 557–560. (doi:10.1038/ngeo1498).
25. Warny S, Askin RA, Hannah MJ, Mohr BAR, Raine JI, Harwood DM, Florindo F, SMS Science Team. 2009 Palynomorphs from a sediment core reveal a sudden remarkably warm Antarctica during the middle Miocene. *Geol. Soc. Am.* **37**, 955–958.
26. Hays JD, Imbrie J, Shackleton NJ. 1976 Variations in the Earth's orbit: pacemaker of the ice ages. *Science* **194**, 1121–1132. (doi:10.1126/science.194.4270.1121)
27. Berger AL. 1978 Long term variations of daily insolation and quaternary climate changes. *J. Atmos. Sci.* **35**, 2362–2367. (doi:10.1175/1520-0469(1978)035<2362:LTVODI>2.0.CO;2)
28. Milankovitch M. 1941 *Kanon der Erdbestrahlung und seine Andwendung auf das Eiszeiten-problem*. Belgrade, Serbia: Royal Serbian Academy.
29. Jouzel J *et al.* 2007 Orbital and millennial Antarctic climate variability over the past 800 000 years. *Science* **317**, 793–796. (doi:10.1126/science.1141038)
30. Kohler P, Bintanja R, Fischer H, Joos F, Knutti R, Lohmann G, Masson-Delmotte V. 2010 What caused Earth's temperature variations during the last 800,000 years? Data-based evidence on radiative forcing and constraints on climate sensitivity. *Quat. Sci. Rev.* **29**, 129–145. (doi:10.1016/j.quascirev.2009.09.026)
31. Masson-Delmoatte V *et al.* 2010 EPICA Dome C record of glacial and interglacial intensities. *Quat. Sci. Rev.* **29**, 113–128. (doi:10.1016/j.quascirev.2009.09.030)
32. Ruddiman WF, Prell WL, Raymo ME. 1989 Late Cenozoic uplift in southern Asia and in the American west: rationale for general circulation model experiment. *J. Geophys. Res.* **94**, 18 409–18 427. (doi:10.1029/JD094iD15p18409)
33. Keigwin LD. 1982 Isotopic paleoceanography of the Caribbean and east Pacific: role of Panama uplift in Late Neogene time. *Science* **217**, 350–352. (doi:10.1126/science.217.4557.350)
34. Kennett J. 1977 Cenozoic evolution of Antarctic glaciation, the circum-Antarctic Ocean, and their impact on global paleoceanography. *J. Geophys. Res.* **82**, 3843–3860. (doi:10.1029/JC082i027p03843)
35. Ramstein G, Fluteau F, Besse J, Joussaume S. 1997 Effect of orogeny, plate motion and land–sea distribution on Eurasian climate change over the past 30 million years. *Nature* **386**, 788–795. (doi:10.1038/386788a0)
36. Lunt DJ, Valdes PJ, Haywood A, Rutt IC. 2008 Closure of the Panama Seaway during the Pliocene: implications for climate and Northern Hemisphere glaciation. *Clim. Dyn.* **30**, 1–18. (doi:10.1007/s00382-007-0265-6)
37. Scher HD, Martin EE. 2006 Timing and climatic consequences of the opening of the Drake Passage. *Science* **312**, 428–430. (doi:10.1126/science.1120044)
38. Urey HC. 1947 The thermodynamic properties of isotopic substances. *J. Chem. Soc.* **1947**, 562–581. (doi:10.1039/jr9470000562)
39. Emiliani C. 1955 Pleistocene temperatures. *J. Geol.* **63**, 538–578. (doi:10.1086/626295)
40. Jaffres JBD, Shileds GA, Wallmann K. 2007 The oxygen isotope evolution of seawater: a critical review of a long-standing controversy and an improved geological water cycle model for the past 3.4 billion years. *Earth Sci. Rev.* **83**, 83–122. (doi:10.1016/j.earscirev.2007.04.002)
41. Wallmann K. 2001 The geological water cycle and the evolution of marine $\delta^{18}O$ values. *Geochim. Cosmochim. Acta* **65**, 2469–2485. (doi:10.1016/S0016-7037(01)00603-2)
42. Cutler KB, Edwards RL, Taylor FW, Cheng H, Adkins J, Gallup CD, Cutler PM, Burr GS, Bloom AL. 2003 Rapid sea-level fall and deep-ocean temperature change since the last interglacial period. *Earth Planet. Sci. Lett.* **206**, 253–271. (doi:10.1016/S0012-821X(02)01107-X)
43. Waelbroeck C *et al.* 2002 Sea-level and deep water temperature changes derived from benthic foraminifera isotopic records. *Quat. Sci. Rev.* **21**, 295–305. (doi:10.1016/S0277-3791(01)00101-9)
44. Fairbanks RG. 1989 A 17,000-year Glacio-Eustatic sea-level record: influence of glacial melting rates on the younger rates on the Younger Dryas event and deep-ocean circulation. *Nature* **342**, 637–642. (doi:10.1038/342637a0)
45. Peltier WR, Fairbanks RG. 2006 Global glacial ice volume and Last Glacial Maximum duration from an extended Barbados sea level record. *Quat. Sci. Rev.* **25**, 3322–3337. (doi:10.1016/j.quascirev.2006.04.010)

46. de Boer B, Van de Wal Bintanja R, Lourens LJ, Tuetter E. 2010 Cenozoic global ice-volume and temperature simulations with 1-D ice-sheet models forced by benthic δ^{18}O records. *Ann. Glaciol.* **51**, 23–33. (doi:10.3189/172756410791392736)
47. Rohling EJ, Grant K, Bolshaw M, Roberts AP, Siddall M, Hemleben C, Kucera M. 2009 Antarctic temperature and global sea level closely coupled over the past five glacial cycles. *Nat. Geosci.* **2**, 500–504. (doi:10.1038/ngeo557)
48. Intergovernmental Panel on Climate Change. 2007 *Climate change 2007: mitigation of climate change* (eds B Metz *et al.*). Cambridge, UK: Cambridge University Press.
49. Hansen JE. 2005 A slippery slope: how much global warming constitutes "dangerous anthropogenic interference"? *Clim. Change* **68**, 269–279. (doi:10.1007/s10584-005-4135-0)
50. Hansen JE. 2007 Scientific reticence and sea level rise. *Environ. Res. Lett.* **2**, 024002. (doi:10.1088/1748-9326/2/2/024002)
51. Overpeck JT, Otto-Bliesner BL, Miller GH, Muhs DR, Alley RB, Kiehl JT. 2006 Paleoclimatic evidence for future ice-sheet instability and rapid sea-level rise. *Science* **311**, 1747–1750. (doi:10.1126/science.1115159)
52. Rohling EJ, Grant K, Hemleben C, Siddall M, Hoogakker BAA, Bolshaw M, Kucera M. 2008 High rates of sea-level rise during the last interglacial period. *Nat. Geosci.* **1**, 38–42. (doi:10.1038/ngeo.2007.28)
53. Kopp RE, Simons FJ, Mitrovica JX, Maloof AC, Oppenheimer M. 2009 Probabilistic assessment of sea level during the last interglacial stage. *Nature* **462**, 863–867. (doi:10.1038/nature08686)
54. Hearty PJ, Kindler P, Cheng H, Edwards RL. 1999 A +20 m middle Pleistocene sea-level highstand (Bermuda and the Bahamas) due to partial collapse of Antarctic ice. *Geology* **27**, 375–378. (doi:10.1130/0091-7613(1999)027<0375:AMMPSL>2.3.CO;2)
55. Hearty PJ. 2010 Comment on "Sea level ~400,000 years ago (MIS 11): analogue for present and future sea level?" by D. Q. Bowen (2010) Can the extrapolation of uplift rates from MIS 5e shorelines to MIS 11 replace direct and tangible evidence of the latter's sea-level history? *Clim. Past Discuss.* **6**, 295–305. (doi:10.5194/cpd-6-295-2010)
56. Rohling EJ, Braun K, Grant K, Kucera M, Roberts AP, Siddall M, Trommer G. 2010 Comparison between Holocene and Marine Isotope Stage-11 sea-level histories. *Earth Planet. Sci. Lett.* **291**, 97–105. (doi:10.1016/j.epsl.2009.12.054)
57. Bowen DQ. 2010 Sea level 400,000 years ago (MIS 11): analogue for present and future sea level? *Clim. Past* **6**, 19–29. (doi:10.5194/cp-6-19-2010)
58. Raymo ME, Mitrovica JX. 2012 Collapse of polar ice sheets during the stage 11 interglacial. *Nature* **483**, 453–456. (doi:10.1038/nature10891)
59. Bintanja R, van de Wal RSW, Oerlemans J. 2005 Modelled atmospheric temperatures and global sea levels over the past million years. *Nature* **437**, 25–128. (doi:10.1038/nature03975)
60. Hansen JE, Sato M. 2012 Paleoclimate implications for human-made climate change. In *Climate change: inferences from paleoclimate and regional aspects* (eds A Berger, F Mesinger, D Šijaèki), pp. 21–48. Vienna, Austria: Springer.
61. Miller KG *et al.* 2012 High tide of the warm Pliocene: implications of global sea level for Antarctic deglaciation. *Geology* **40**, 407–410. (doi:10.1130/G32869.1)
62. Lear CH, Elderfield H, Wilson PA. 2000 Cenozoic deep-sea temperatures and global ice volumes from Mg/Ca in benthic foraminiferal calcite. *Science* **287**, 269–272. (doi:10.1126/science.287.5451.269)
63. Dowsett HJ, Barron JA, Poore RZ, Thompson RS, Cronin TM, Ishman SE, Willard DA. 1999 Middle Pliocene paleoenvironmental reconstruction: PRISM 2. *US Geol. Survey Open File Rep.* **236**, 99–535.
64. Dwyer GS, Chandler MA. 2009 Mid-Pliocene sea level and continental ice volume based on coupled benthic Mg/Ca palaeotemperatures and oxygen isotopes. *Phil. Trans. R. Soc. A* **367**, 157–168. (doi:10.1098/rsta.2008.0222)
65. Raymo ME, Mitrovica JX, O'Leary MJ, DeConto RM, Hearty PJ. 2011 Departures from eustasy in Pliocene sea-level records. *Nat. Geosci.* **4**, 328–332. (doi:10.1038/ngeo1118)
66. Hansen J *et al.* 2005 Efficacy of climate forcings. *J. Geophys. Res.* **110**, D18104. (doi:10.1029/2005JD005776)
67. Haywood AM *et al.* 2010 Pliocene Model Intercomparison Project (PlioMIP): experimental design and boundary conditions (experiment 1). *Geosci. Model Dev.* **3**, 227–242. (doi:10.5194/gmd-3-227-2010)

68. Haywood AM *et al.* 2012 Large scale features of the Pliocene climate: results from the Pliocene Model Intercomparison Project. *Clim. Past Discuss.* **8**, 2969–3013. (doi:10.5194/cpd-8-2969-2012)
69. Jones PD, New M, Parker DE, Martin S, Rigor IG. 1999 Surface air temperature and its variations over the last 150 years. *Rev. Geophys.* **37**, 173–199. (doi:10.1029/1999RG900002)
70. Hansen J, Ruedy R, Sato M, Lo K. 2010 Global surface temperature change. *Rev. Geophys.* **48**, RG4004. (doi:10.1029/2010RG000345)
71. Mayewski PA *et al.* 2004 Holocene climate variability. *Quat. Res.* **62**, 243–255. (doi:10.1016/j.yqres.2004.07.001)
72. Nerem RS, Leuliette E, Casanave A. 2006 Present-day sea-level change: a review. *C. R. Geosci.* **338**, 1077–1083. (doi:10.1016/j.crte.2006.09.001)
73. Rignot E, Velicogna I, van den Broeke MR, Monaghan A, Lenaerts J. 2011 Acceleration of the contribution of the Greenland and Antarctic ice sheets to sea level rise. *Geophys. Res. Lett.* **38**, L05503. (doi:10.1029/2011GL046583)
74. King MA, Bingham RJ, Moore P, Whitehouse PL, Bentley MJ, Milne GA. 2012 Lower satellite-gravimetry estimates of Antarctic sea-level contribution. *Nature* **491**, 586–589. (doi:10.1038/nature11621)
75. Zwally HJ *et al.* 2011 Greenland ice sheet mass balance: distribution of increased mass loss with climatic warming: 2003–07 versus 1992–2002. *J. Glaciol.* **57**, 1–15. (doi:10.3189/002214311795306682)
76. Clark PU, Huybers P. 2009 Interglacial and future sea level. *Nature* **462**, 8567–8857. (doi:10.1038/462856a)
77. McKay NP, Overpeck JT, Otto-Bliesner BL. 2011 The role of ocean thermal expansion in Last Interglacial sea level rise. *Geophys. Res. Lett.* **38**, L14605. (doi:10.1029/2011GL048280)
78. Turney CSM, Jones RT. 2010 Does the Agulhas current amplify global temperatures during super-interglacials? *J. Quat. Sci.* **25**, 839–843. (doi:10.1002/jqs.1423)
79. Zachos JC, Schouten S, Bohaty S, Quattlebaum T, Sluijs A, Brinkhuis H, Gibbs SJ, Bralower TJ. 2006 Extreme warming of id-latitude coastal ocean during the Paleocene–Eocene thermal maximum: inferences from TEX_{86} and isotope data. *Geol. Soc. Am.* **34**, 737–740.
80. Pearson PN, van Dongen BE, Nicholas CJ, Pancost RD, Schouten S, Singano JM, Wade BS. 2007 Stable warm tropical climate through the Eocene Epoch. *Geology* **35**, 211–214. (doi:10.1130/G23175A.1)
81. Hollis CJ *et al.* 2009 Tropical sea temperatures in the high-latitude South Pacific during the Eocene. *Geology* **37**, 99–102. (doi:10.1130/G25200A.1)
82. Hollis CJ *et al.* 2012 Early Paleogene temperature history of the Southwest Pacific Ocean: reconciling proxies and models. *Earth Planet. Sci. Lett.* **349**, 53–56. (doi:10.1016/j.epsl.2012.06.024)
83. Lunt DJ *et al.* 2012 A model-data comparison for a multi-model ensemble of Early Eocene atmosphere–ocean simulations: EoMIP. *Clim. Past* **8**, 1717–1736. (doi:10.5194/cp-8-1717-2012)
84. Bijl PK, Schouten S, Sluijs A, Reichart GJ, Zachos JC, Brinkhuis H. 2009 Early Palaeogene temperature evolution of the Southwest Pacific Ocean. *Nature* **461**, 776–779. (doi:10.1038/nature08399)
85. Colman R, McAvaney B. 2009 Climate feedbacks under a broad range of forcing. *Geophys. Res. Lett.* **36**, L01702. (doi:10.1029/2008GL036268)
86. Lorius C, Jouzel J, Raynaud D, Hansen J, Letreut H. 1990 The ice-core record: climate sensitivity and future greenhouse warming. *Nature* **347**, 139–145. (doi:10.1038/347139a0)
87. Luthi D *et al.* 2008 High-resolution carbon dioxide concentration record 650,000–800,000 years before present. *Nature* **453**, 379–382. (doi:10.1038/nature06949)
88. Loulergue L *et al.* 2008 Orbital and millennial-scale features of atmospheric CH_4 over the past 800,000 years. *Nature* **453**, 383–386. (doi:10.1038/nature06950)
89. Hansen J, Sato M, Ruedy R, Lacis A, Oinas V. 2000 Global warming in the twenty-first century: an alternative scenario. *Proc. Natl Acad. Sci. USA* **97**, 9875–9880. (doi:10.1073/pnas.170278997)
90. Spahni R *et al.* 2005 Atmospheric methane and nitrous oxide of the late Pleistocene from Antarctic ice cores. *Science* **310**, 1317–1321. (doi:10.1126/science.1120132)
91. Hansen J, Sato M, Kharecha P, Russell G, Lea DW, Siddall M. 2007 Climate change and trace gases. *Phil. Trans. R. Soc. A* **365**, 1925–1954. (doi:10.1098/rsta.2007.2052)

92. Hansen J, Russell G, Rind D, Stone P, Lacis A, Lebedeff S, Ruedy R, Travis L. 1983 Efficient three-dimensional global models for climate studies: models I and II. *Mon. Weather Rev.* **111**, 609–662. (doi:10.1175/1520-0493(1983)111<0609:ETDGMF>2.0.CO;2)
93. Hewitt C, Mitchell J. 1997 Radiative forcing and response of a GCM to ice age boundary conditions: cloud feedback and climate sensitivity. *Clim. Dyn.* **13**, 821–834. (doi:10.1007/s003820050199)
94. Schmittner A, Urban NM, Shakun JD, Mahowald NM, Clark PU, Bartlein PJ, Mix AC, Rosell-Melé A. 2011 Climate sensitivity estimated from temperature reconstructions of the Last Glacial Maximum. *Science* **334**, 1385–1388. (doi:10.1126/science.1203513)
95. Schneider von Deimling T, Ganopolski A, Held H, Rahmstorf S. 2006 How cold was the Last Glacial Maximum? *Geophys. Res. Lett.* **33**, L14709. (doi:10.1029/2006GL026484)
96. CLIMAP Project, McIntyre A. 1981 *Seasonal reconstruction of Earth's surface at the Last Glacial Maximum*. Map and Chart Series, No. 36. Boulder, CO: Geological Society of America.
97. Dowsett HJ, Robinson MM, Foley KM. 2009 Pliocene three-dimensional global ocean temperature reconstruction. *Clim. Past* **5**, 700–783.
98. Dowsett HJ *et al.* 2010 The PRISM3D paleoenvironmental reconstruction. *Stratigraphy* **7**, 123–139.
99. PALAEOSENS Project Members, Rohling EJA *et al.* 2012 Making sense of palaeoclimate sensitivity. *Nature* **491**, 683–691. (doi:10.1038/nature11574)
100. Budyko MI. 1969 The effect of solar radiation variations on the climate of the Earth. *Tellus* **21**, 611–619. (doi:10.1111/j.2153-3490.1969.tb00466.x)
101. Pierrehumbert RT, Abbot DS, Voigt A, Koll D. 2011 Climate of the Neoproterozoic. *Annu. Rev. Earth Planet. Sci.* **39**, 417–460. (doi:10.1146/annurev-earth-040809-152447)
102. Kirschvink JL. 1992 Late Proterozoic low-latitude global glaciation: the snowball earth. In *The Proterozoic biosphere* (eds JW Schopf, C Klein), pp. 51–52. Cambridge, UK: Cambridge University Press.
103. Hoffman PF, Schrag DP. 2002 The snowball Earth hypothesis: testing the limits of global change. *Terra Nova* **14**, 129–155. (doi:10.1046/j.1365-3121.2002.00408.x)
104. Tyndall J. 1861 On the absorption and radiation of heat by gases and vapours. *Lond. Edinb. Dublin Phil. Mag.* **22**, 169–194.
105. Ingersoll AP. 1969 Runaway greenhouse: a history of water on Venus. *J. Atmos. Sci.* **26**, 1191–1198. (doi:10.1175/1520-0469(1969)026<1191:TRGAHO>2.0.CO;2)
106. Kasting JF. 1988 Runaway and moist greenhouse atmospheres and the evolution of Earth and Venus. *Icarus* **74**, 472–494. (doi:10.1016/0019-1035(88)90116-9)
107. Donahue TM, Hoffman JH, Hodges RR, Watson AJ. 1982 Venus was wet: a measurement of the ratio of deuterium to hydrogen. *Science* **216**, 630–633. (doi:10.1126/science.216.4546.630)
108. Russell GL, Miller JR, Rind D. 1995 A coupled atmosphere–ocean model for transient climate change studies. *Atmos. Ocean* **33**, 683–730. (doi:10.1080/07055900.1995.9649550)
109. Russell G. 2007 Step-mountain technique applied to an atmospheric C-grid model, or how to improve precipitation near mountains. *Mon. Weather Rev.* **135**, 4060–4076. (doi:10.1175/2007MWR2048.1)
110. Lacis AA, Oinas V. 1991 A description of the correlated k distributed method for modeling nongray gaseous absorption, thermal emission, and multiple scattering in vertically inhomogeneous atmospheres. *J. Geophys. Res.* **96**, 9027–9063. (doi:10.1029/90JD01945)
111. Hansen J, Sato M, Ruedy R. 1997 Radiative forcing and climate response. *J. Geophys. Res.* **102**, 6831–6864. (doi:10.1029/96JD03436)
112. Russell GL, Rind DH, Colose C, Lacis AA, Opstbaum RF. Fast atmosphere-ocean model run with large changes in CO_2. Submitted to Geophys. Res. Lett.
113. Hoffman PF, Li ZX. 2009 A palaeogeographic context for Neoproterozoic glaciation. *Palaeogeogr. Palaeoclim. Palaeoecol.* **277**, 158–172. (doi:10.1016/j.palaeo.2009.03.013)
114. Global Energy Assessment. 2012 *Toward a sustainable future* (eds TB Johanson *et al.*). Laxenburg, Austria: International Institute for Applied Systems Analysis.
115. Kenney WL, DeGroot DW, Holowatz LA. 2004 Extremes of human heat tolerance: life at the precipice of thermoregulatory failure. *J. Therm. Biol.* **29**, 479–485. (doi:10.1016/j.jtherbio.2004.08.017)
116. Hanna JM, Brown DE. 1983 Human heat tolerance: an anthropological perspective. *Annu. Rev. Anthropol.* **12**, 259–284. (doi:10.1146/annurev.an.12.100183.001355)
117. Kasting JF, Donahue TM. 1980 The evolution of the atmospheric ozone. *J. Geophys. Res.* **85**, 3255–3263. (doi:10.1029/JC085iC06p03255)

118. Lunt DJ, Haywood AM, Schmidt GA, Salzmann U, Valdes PJ, Dowsett HJ. 2010 Earth system sensitivity inferred from Pliocene modelling and data. *Nat. Geosci.* **3**, 60–64. (doi:10.1038/ngeo706)
119. Pagani M, Liu ZH, LaRiviere J, Ravelo AC. 2010 High Earth-system climate sensitivity determined from Pliocene carbon dioxide concentrations. *Nat. Geosci.* **3**, 27–30. (doi:10.1038/ngeo724)
120. Royer DL, Pagani M, Beerling DJ. 2012 Geobiological constraints on Earth system sensitivity to CO_2 during the Cretaceous and Cenozoic. *Geobiology* **10**, 298–310. (doi:10.1111/j.1472-4669.2012.00320.x)
121. Sackmann IJ, Boothroyd AI, Kraemer KE. 1993 Our sun III: present and future. *Astrophys. J.* **418**, 457–468. (doi:10.1086/173407)
122. Beerling DJ, Fox A, Stevenson DS, Valdes PJ. 2011 Enhanced chemistry-climate feedbacks in past greenhouse worlds. *Proc. Natl Acad. Sci. USA* **108**, 9770–9775. (doi:10.1073/pnas.1102409108)
123. van de Wal RSW, de Boer B, Lourens LJ, Kohler P, Bintanja R. 2011 Reconstruction of a continuous high-resolution CO_2 record over the past 20 million years. *Clim. Past* **7**, 1459–1469. (doi:10.5194/cp-7-1459-2011)
124. Pollard D, DeConto RM. 2005 Hysteresis in Cenozoic Antarctic ice-sheet variations. *Glob. Planet. Change* **45**, 9–21. (doi:10.1016/j.gloplacha.2004.09.011)
125. John CM, Karner GD, Browning E, Leckie RM, Mateo Z, Carson B, Lowery C. 2011 Timing and magnitude of Miocene eustasy derived from the mixed siliciclastic-carbonate stratigraphic record of the northeastern Australian margin. *Earth Planet. Sci. Lett.* **304**, 455–467. (doi:10.1016/j.epsl.2011.02.013)
126. Nurnberg D, Muller A, Schneider RR. 2000 Paleo-sea surface temperature calculations in the equatorial East Atlantic from Mg/Ca ratios in planktic foraminifera: a comparison to sea surface temperature estimates from $U^{K'}_{37}$, oxygen isotopes, and foraminiferal transfer function. *Paleoceanography* **15**, 124–134. (doi:10.1029/1999PA000370)
127. Ruddiman WF. 2003 The anthropogenic greenhouse era began thousands of years ago. *Clim. Change* **61**, 261–293. (doi:10.1023/B:CLIM.0000004577.17928.fa)
128. Goldblatt C, Watson AJ. 2012 The runaway greenhouse: implications for future climate change, geoengineering and planetary atmospheres. *Phil. Trans. R. Soc. A* **370**, 4197–4216. (doi:10.1098/rsta.2012.0004)
129. Archer D *et al.* 2009 Atmospheric lifetime of fossil fuel carbon dioxide. *Annu. Rev. Earth Planet. Sci.* **37**, 117–134. (doi:10.1146/annurev.earth.031208.100206)
130. Hatfield JL, Boote KJ, Kimball BA, Ziska LH, Izaurralde RC, Ort D, Thomson AM, Wolfe D. 2011 Climate impacts on agriculture: implications for crop production. *Agron. J.* **103**, 351–370.
131. Anderson JG, Wilmouth DM, Smith JB, Sayres DS. 2012 UV dosage levels in summer: increased risk of ozone loss from convectively injected water vapor. *Science* **337**, 835–839. (doi:10.1126/science.1222978)
132. Sherwood SC, Huber M. 2010 An adaptability limit to climate change due to heat stress. *Proc. Natl Acad. Sci. USA* **107**, 9552–9555. (doi:10.1073/pnas.0913352107)
133. McMichael AJ, Dear KB. 2010 Climate change: heat, health, and longer horizons. *Proc. Natl Acad. Sci. USA* **107**, 9483–9484. (doi:10.1073/pnas.1004894107)
134. Dewhirst MW, Viglianti BL, Lora-Michiels M, Hanson M, Hoopes PJ. 2003 Basic principles of thermal dosimetry and thermal thresholds for tissue damage from hyperthermia. *Int. J. Hypertherm.* **19**, 267–294. (doi:10.1080/0265673031000119006)
135. Kjellstrom T, Holmer I, Lemke B. 2009 Workplace heat stress, health and productivity—an increasing challenge for low and middle-income countries during climate change. *Glob. Health Action*. (doi:10.3402/gha.v2i0.2047)
136. Alroy J, Koch PL, Zachos JC. 2000 Global climate change and North American mammalian evolution. *Paleobiology* **26**, 259–288. (doi:10.1666/0094-8373(2000)26[259:GCCANA]2.0.CO;2)
137. Smith JJ, Haslotis ST, Kraus MJ, Woody DT. 2004 Transient dwarfism of soil fauna during the Paleocene–Eocene Thermal Maximum. *Proc. Natl Acad. Sci. USA* **106**, 17 655–17 660. (doi:10.1073/pnas.0909674106)
138. Masson-Delmotte V *et al.* 2011 Sensitivity of interglacial Greenland temperature and $\delta^{18}O$: ice core data, orbital and increased CO_2 climate simulations. *Clim. Past* **7**, 1041–1059. (doi:10.5194/cp-7-1041-2011)